SSC-219

CRACK PROPAGATION AND ARREST IN SHIP AND OTHER STEELS

SHIP STRUCTURE COMMITTEE

1971

SHIP STRUCTURE COMMITTEE

AN INTERAGENCY ADVISORY
COMMITTEE DEDICATED TO IMPROVING
THE STRUCTURE OF SHIPS

MEMBER AGENCIES:

UNITED STATES COAST GUARD
NAVAL SHIP SYSTEMS COMMAND
MILITARY SEALIFT COMMAND
MARITIME ADMINISTRATION
AMERICAN BUREAU OF SHIPPING

ADDRESS CORRESPONDENCE TO:

SECRETARY
SHIP STRUCTURE COMMITTEE
U.S. COAST GUARD HEADQUARTERS
WASHINGTON, D.C. 20591

SR 180
1971

6 AUG 1971

The Ship Structure Committee is sponsoring research in the application of modern experimental techniques to the brittle fracture of ship plates. This report describes experiments in crack initiation, propagation and arrest. Additional work in this area is being undertaken. The possible development of a crack arrest criterion is indicated.

Comments on this report are solicited.

W. F. REA III
Rear Admiral, U. S. Coast Guard
Chairman, Ship Structure Committee

SSC-119
Final Report
on
Project SR-180, "Fracture-Strain Program"

to the

Ship Structure Committee

CRACK PROPAGATION AND ARREST IN SHIP AND OTHER STEELS

by

G. T. Hahn, R. G. Hoagland, P. N. Mincer,
A. R. Rosenfield, and M. Sarrate
Battelle Memorial Institute

under
Department of the Navy
Naval Ship Engineering Center
Contract No. N00024-68-C-5073

U. S. Coast Guard Headquarters
Washington, D.C.
1971

ABSTRACT

This report describes a three-part investigation into the major stages of fracture--initiation, propagation, and arrest. To study all aspects of the problem, a wedge-loaded double-cantilever-beam design was used because of its crack arrest capability. Much of the experimentation was done on Fe-3Si Steel where crack-tip yielding can be revealed by a special etching technique. Additionally, a number of experiments were done on engineering steels, principally to study propagation resistance.

The specimen and the plastic zones produced prior to crack initiation are first described and compared with analytical and experimental results in the literature, for purposes of calibration. The mechanism of cleavage crack propagation was then investigated. It was found that the fast moving crack bypasses some of the grains as it grows, leaving behind unbroken ligaments. Rupture of these ligaments consumes a large amount of energy locally and this process can account for crack propagation resistance values estimated from these experiments.

Upon increasing root radius of the initial notch,the crack must be overloaded to propagate, and a wide range of values of the crack driving force, G, can be obtained in a single experiment. This provides a new method of measuring crack propagation resistance, R. Etching results suggest that R does not vary greatly as the crack grows. An energy balance shows that R is the average value of G during propagation. By this means, partial confirmation is given to the idea that R is equal to the value of G_{Ic} measured in an impact test. It is then shown that the rate and temperature dependence of $K_{Ic} = (EG_{Ic})^{1/2}$ arises from the rate and temperature dependence of the yield stress in the crack-tip plastic zone.

These analyses and experiments provide a framework for developing a practical arrest criterion for ship steels.

CONTENTS

SHIP STRUCTURE COMMITTEE

The SHIP STRUCTURE COMMITTEE is constituted to prosecute a research program to improve the hull structures of ships by an extension of knowledge pertaining to design, materials and methods of fabrication.

RADM W. F. Rea, III, USCG, Chairman
Chief, Office of Merchant Marine Safety
U. S. Coast Guard Headquarters

Capt. J. E. Rasmussen
Naval Ship Engineering Center
Prince Georges'Center Building

Capt. T. J. Banvard, USN
Maintenance and Repair Officer
Military Sealift Command

Mr. E. S. Dillon
Chief
Office of Ship Construction
Maritime Administration

Mr. K. D. Morland, Vice President
American Bureau of Shipping

SHIP STRUCTURE SUBCOMMITTEE

The SHIP STRUCTURE SUBCOMMITTEE acts for the Ship Structure Committee on technical matters by providing technical coordination for the determination of goals and objectives of the program, and by evaluating and interpreting the results in terms of ship structural design, construction and operation.

NAVAL SHIP ENGINEERING CENTER

Mr. P. M. Palermo - Chairman
Mr. J. B. O'Brien - Contract Administrator
Mr. G. Sorkin - Member
Mr. H. S. Sayre - Alternate
Mr. I. Fioriti - Alternate

MARITIME ADMINISTRATION

Mr. F. Dashnaw - Member
Mr. A. Maillar - Member
Mr. R. Falls - Alternate
Mr. Raymond F. Coombs - Alternate

AMERICAN BUREAU OF SHIPPING

Mr. S. G. Stiansen - Member
Mr. F. J. Crum - Member

OFFICE OF NAVAL RESEARCH

Mr. J. M. Crowley - Member
Dr. W. G. Rauch - Alternate

NAVAL SHIP RESEARCH & DEVELOPMENT CENTER

Mr. A. B. Stavovy - Alternate

MILITARY SEALIFT COMMAND

Mr. R. R. Askren - Member
LT.JG. E. T. Powers, USNR - Member

U. S. COAST GUARD

LCDR C. S. Loosmore, USCG, Secretary
CDR C. R. Thompson, USCG - Member
CDR J. W. Kime, USCG - Alternate
CDR J. L. Coburn - Alternate

NATIONAL ACADEMY OF SCIENCES

Mr. R. W. Rumke, Liaison
Prof. R. A. Yagle, Liaison

SOCIETY OF NAVAL ARCHITECTS & MARINE ENGINEERS

Mr. T. M. Buermann, Liaison

BRITISH NAVY STAFF

Dr. V. Flint, Liaison
CDR P. H. H. Ablett, RCNC, Liaison

WELDING RESEARCH COUNCIL

Mr. K. H. Koopman, Liaison
Mr. C. Larson, Liaison

LIST OF ILLUSTRATIONS

LIST OF ILLUSTRATIONS (Cont.)

LIST OF TABLES

INTRODUCTION

With the trend toward higher strength steels and more highly stressed ship hulls, more precautions must be taken to guard against fracture. Existing methods already make it possible to identify safe stress-level/flaw-size combinations, provided the flaw is imbedded in material of standard quality. However, this is not the only source of failure. A more likely source is a crack located in an atypical region of low toughness (like the HAZ of a weld). Such a flaw will become unstable and begin to propagate at even lower stress levels. The question then is: will the crack emerging from the "bad region be arrested when it reaches the "good (standard quality) material that surrounds it? The concept of designing for crack arrest is not new. Pellini and his coworkers at NRL[1] have for some years advocated a "crack arrest" philosophy. What is needed now is a more precise description of steels' arrest capabilities--something like Pellini's FAD (Fracture Analysis Diagram), but in terms of the length of running crack that can be arrested at different stress levels by the base metal and by continuous weld-affected regions.

This program was undertaken to explore the possibility of measuring and analyzing crack propagation and arrest. These processes depend on a number of factors: (1) the mechanics of the flawed structure (or test specimen), (2) the plastically deformed zone at the crack tip, (3) the metal's resistance to plastic flow and its rate dependence, and (4) the processes of cleavage and ductile rupture on the microstructural scale. The work sought numerical descriptions of the individual factors with the aim of assembling these into a comprehensive, systems-type analysis of propagation and arrest.

The studies employed the DCB (double-cantilever-beam) test specimen because this configuration offers the possibility of initiating, propagating, and arresting a fast fracture, under controlled conditions, within the confines of a single specimen. Analyses of the stress fields of stationary cracks in DCB specimens are reported in the literature. A flexible, one-dimensional analysis of a crack propagating in a DCB specimen has recently been devised by M. F. Kanninen of Battelle-Columbus under separate sponsorship. Section 1 of this report deals with the plastic zones produced by stationary cracks in this type of specimen. This work, which exploits the Fe-3Si etching technique, was undertaken to establish a base line for comparisons with zones produced by moving cracks.

Section 2 describes experiments which simulate slowly moving cracks. This work revealed that the deformed material, left behind by an advancing crack tip has relatively little influence on the stress field ahead of the crack, at least under plane strain conditions--a result which simplifies the interpretation of propagating cracks. The work described in Section 2 also demonstrates the advantages of the DCB specimen for studies of fast fracture arrest. Under wedge loading, fast fractures travel in essentially a straight line into a continuously decreasing stress field and finally arrest. Metallographic sections of the arrested fractures reveal that isolated, unbroken ligaments are left behind by the advancing crack front. The etching studies show clearly, for the first time, that the stretching of these ligaments behind the crack front is the main source of energy dissipation by plastic flow during propagation.

With these results in hand, the research described in Section 3 turned to quantitative studies of the relations between the stress intensity (K) levels at initiation and arrest in a variety of steels. The method of estimating $\bar{R}_d$, the average energy absorption rate of a propagating fracture, from the stress intensity values at initiation and arrest is discussed. Experiments in which the acuity of the starting notch was varied show that K(arrest) decreases as the K(initiation) is increased consistent with $\bar{R}_d$-value close to the value of G_{Ic}. Accordingly, the arrest condition depends on the stress and flaw size at initiation, the geometry of the specimen, and $\bar{R}_d$, and is not an invariant. In the present experiments, the ratio of K(initiation) to K(arrest) varied from $\sim$ 1 to $\sim$ 4. Detailed metallographic studies show that the ligament mechanism of crack propagation occurs in all steels studied. By sectioning several samples, it was found that the ligaments are of limited thickness and that they are isolated regions bypassed by the crack. Using this idea, a model of dynamic crack resistance is proposed, in which the stress intensity at the crack tip is diminished by the effect of the ligaments which are believed to support a stress on the order of the yield stress.

In overall terms, the study encourages the view that the crack propagation characteristics of steels can be measured, analyzed, and ultimately used to control fracture arrest. This is illustrated in Figure 1 by an example, the case of a large plate loaded in tension. The example presupposes that a crack in a "bad" region of the plate becomes unstable, propagates a short distance, and then is arrested by base metal characterized by a relatively large value of the average energy absorption rate, $\bar{R}_d$. Stress levels and the size of "bad" regions that can be tolerated can be estimated in this way. Crack arrest may thus offer a more conservative approach to fracture safety, both from the viewpoints of design, inspection, and repair. However, both the experimental and analytical techniques need to be developed more extensively. In addition, the metallurgical factors governing arrest toughness need to be understood for the purposes of alloy development.

Reference

1. W. S. Pellini and P. P. Puzak, "Fracture Analysis Program Procedures for the Fracture-Safe Engineering Design of Steel Structures", NRL Report 5920, March 15, 1963.

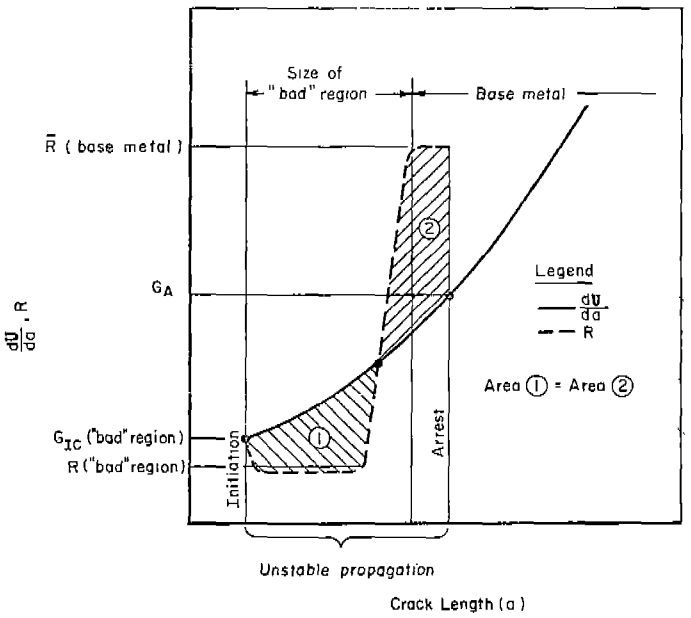

Fig.1. SCHEMATIC REPRESENTATION OF THE ENERGY CHANGES IN A LARGE PLATE UNDER UNIFORM TENSION FOLLOWING THE INITIATION OF A CRACK IN A "BAD" REGION AND ITS ARREST BY THE BASE METAL SURROUNDING IT. HERE U REPRESENTS THE ELASTIC STRAIN ENERGY STORED IN THE PLATE.

SECTION 1

PLASTIC ZONES IN Fe-3Si STEEL DOUBLE-CANTILEVER-BEAM SPECIMENS

by

G. T. Hahn, M. Sarrate, and A. R. Rosenfield

ABSTRACT

Plastic zones generated in double-cantilever-beam specimens of an Fe-3Si steel are revealed by etching. Zones corresponding to relative stress intensity levels in the range $0.4\ \sqrt{\text{in.}} < \frac{K}{\sigma_Y} < 0.8\ \sqrt{\text{in.}}$, beam height to length ratios $\frac{H}{W} = 0.125$ and 0.35, and conditions approaching $\left(\frac{K}{\sigma_Y}\right)^2$ plane strain are examined. The furthest extent of the zones, $\rho \simeq 0.13 \left(\frac{K}{\sigma_Y}\right)^2$, is about half that previously observed in plates loaded in tension to comparable K-levels. The results are consistent with previous measurements by Clark and lend support to Wilson's calculations. At high stress levels, when the zone size to beam height ratio $\frac{\rho}{H} \gtrsim 0.09$, the zone begins to tilt backwards and undergoes a transition from a crack- to a beam-zone. Implications of this transition with respect to the minimum beam height requirement are examined.

PLASTIC ZONES IN Fe-3Si STEEL DOUBLE-CANTILEVER-BEAM SPECIMENS

I. INTRODUCTION

In view of the many applications for the DCB (double-cantilever-beam) test specimen*, more complete characterizations of this configuration are desirable.[1,2] Such features as size limitations, thickness requirements, and plasticity corrections are of interest, and these depend on the extent and distribution of the plastic deformation generated by a crack in the specimen. A limited study of plastic zones in DCB specimens has been conducted by Clark[3] using the Fe-3Si etching technique. His results are summarized in Figure 1 and indicate that the maximum extent of the DCB zones is about half of that displayed by zones produced by comparable stress field intensity levels in plates under uniform tensile loading.[4] This result receives support from Wilson[5] who has estimated enclave sizes and shapes from the elastic fields obtained by applying boundary collocation to the Williams stress function[6] for a number of specimen configurations. These calculations also show that the infinite plate-uniaxial tension plastic zone is about twice as large as the DCB zone, at least at one stress level.** However, the underlying differences in the elastic field tend to disappear as the crack tip is approached. Wilson also finds a progressive change in the dominant inclination of the enclave, from one that leads to one that trails the crack tip, as the beam height of the specimen is reduced (see Figure 2).

The present study, part of an investigation of the plasticity attending cracks growing under load[7,8], offers more observations of zones in DCB-specimens with a geometry somewhat different from that employed by Clark. The results tend to confirm Clark's findings about zone size, and afford a critical test of Wilson's enclave shape calculations.

---

* Also referred to as the wedge-opening loading (WOL), compact tension (CT), and crack line loaded specimen.

** Wilson offers comparisons at a stress level corresponding to nominal stress-to-yield stress ratio $\sigma/\sigma_Y = 0.36$. The differences among the zones should disappear as $\sigma/\sigma_Y \to 0$.[3]

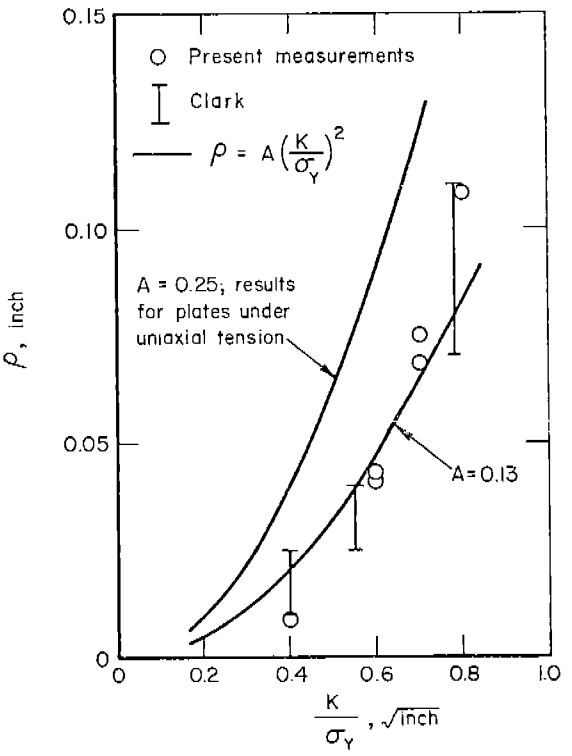

Fig.1. INFLUENCE OF THE RELATIVE STRESS INTENSITY LEVEL ON THE PLASTIC ZONE SIZE OF DCB SPECIMENS. Data points for zones revealed on the mid-section of Series P specimens are compared with Clark's [3] results for DCB specimens and previous measurements on edge and center notched plates in uniaxial tension.[4]

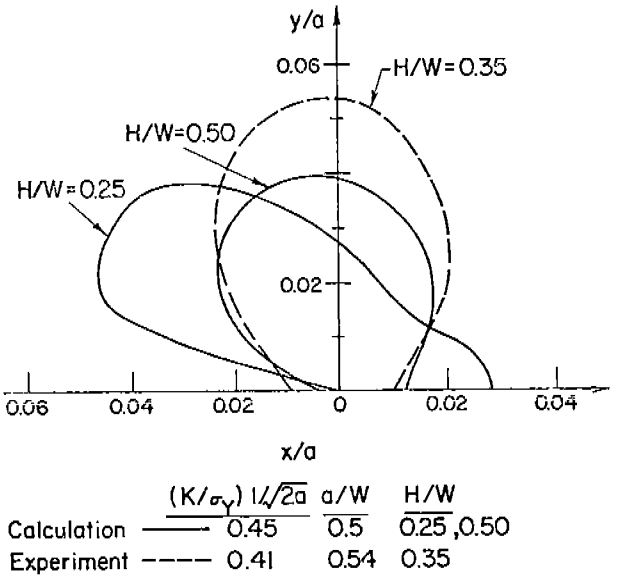

Fig.2. COMPARISON OF PLASTIC ZONES CALCULATED BY WILSON[5] WITH OUTLINE OF ZONE REVEALED BY ETCHING (Spec. 3P-23, $\left(\frac{K}{\sigma_Y}\right) = 0.8\sqrt{\text{in.}}$)

II. EXPERIMENTAL PROCEDURES

The results reported here are for DCB Specimens having the geometry shown in Figure 3 (Series P), and for two specimens with the same length and thickness but a beam height of 0.5 in. (Series A). These two configurations have beam height to length rations, $\frac{H}{W}$ = 0.35 and 0.125, respectively, compared to the ratio $\frac{H}{W}$ = 0.45 employed by Clark. Another difference is that the specimens used here contained spark machined slits cut with 0.005 in.-diameter wire which produced a slit root radius ~ 0.005 in., rather than sharp cracks.*** While the deformation within a root radius of the slit tip is therefore not characteristic of the zone of a crack, portions of the zone at a distance greater than 2-3 root radii from the slit tip are

*** This was done to make the zones comparable to those produced in simulated crack growth experiments [7,8] discussed in the next section of the report.

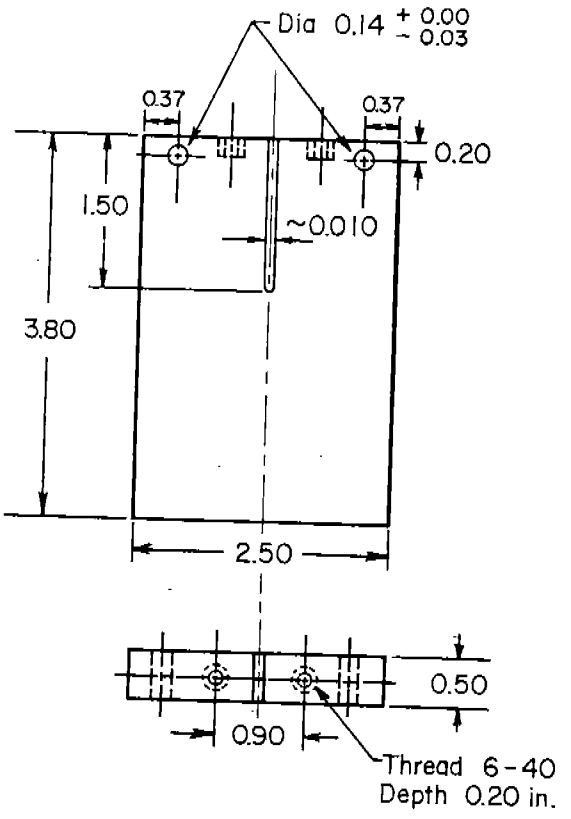

Fig.3. DOUBLE-CANTILEVER-BEAM SPECIMEN

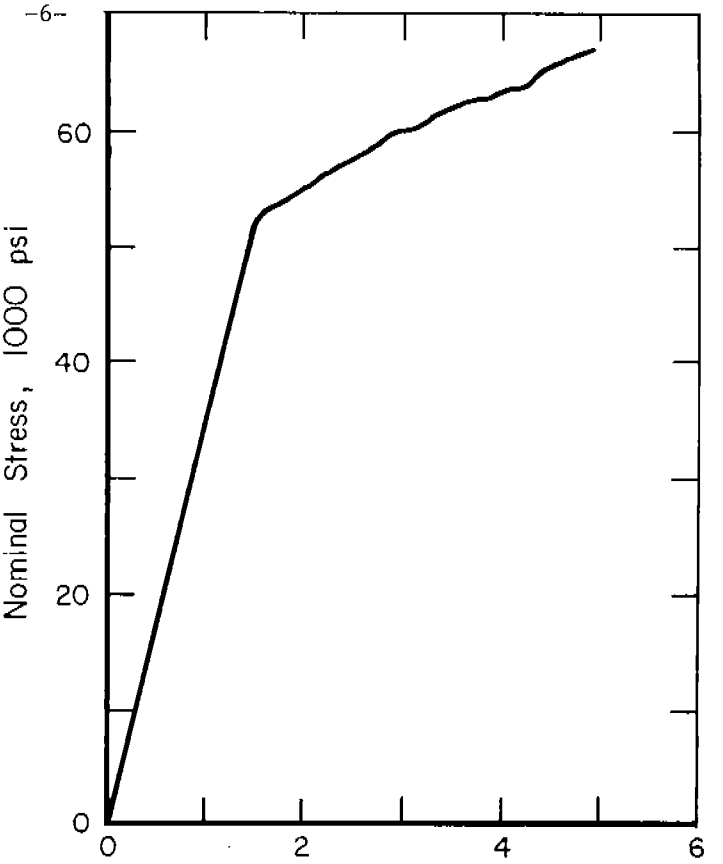

Fig.4. STRESS-STRAIN CHARACTERISTICS OF LOT P Fe-3Si STEEL AT 100°C

probably indistinguishable from those of a sharp crack. The zone size to thickness[7] ratios examined favor a close approach to plane strain conditions and this is discussed more fully in the next section.

The DCB specimens were fabricated from Fe-3Si Steel, annealed, aged, polished, and etched according to procedures described in detail in Reference 9. Series A specimens were tested at room temperature and displayed a yield stress of 65,000 psi. Series P specimens were tested at 100°C to facilitate comparisons with crack growth experiments made at this temperature to avoid cleavage. Lot P displayed a yield stress of 53,500 psi at 100°C and some evidence of strain aging, but not enough to significantly affect the stress-strain curve (shown in Figure 4) during the time the specimens were under load. The specimens were stressed in a horizontal loading device and both the load and the slit opening were monitored (the latter with a displacement gage). Loads were applied and released relatively slowly, at about 5,000 lbs. per minute. In one case, a number of zones were produced in a single specimen by extending the slit after each load-unload cycle and then reloading to a different K-level. Compliance values calculated from the Kanninen[10] equation agree reasonably well with the actual measurements as shown in Figure 5. Plastic zones generated at various K-levels were revealed on the DCB surface and midsection by etching.

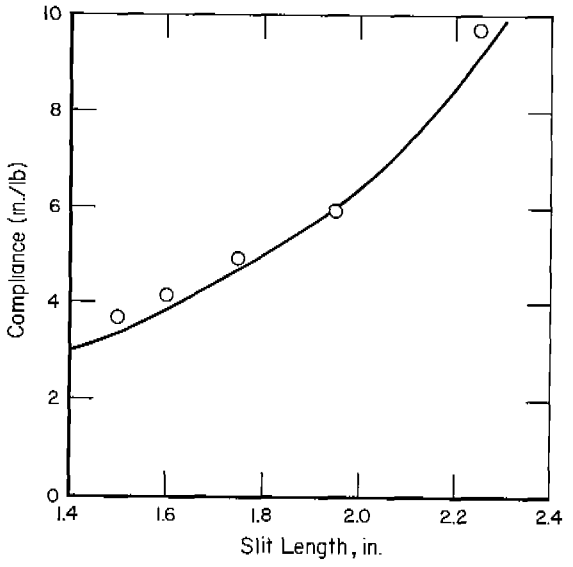

$$C = \frac{4}{Et\lambda^3 H^3}\left[2\lambda^3 a^3 + 6\lambda^2 a^2\left(\frac{\sinh\lambda c\,\cosh\lambda c + \sin\lambda c\,\cos\lambda c}{\sinh^2\lambda c - \sin^2\lambda c}\right) + \right.$$

$$\left. + 6\lambda a\left(\frac{\sinh^2\lambda c + \sin^2\lambda c}{\sinh^2\lambda c - \sin^2\lambda c}\right) + 3\left(\frac{\sinh\lambda c\,\cosh\lambda c - \sin\lambda c\,\cos\lambda c}{\sinh^2\lambda c - \sin^2\lambda c}\right)\right]$$

(See Table 1 for explanation of symbols)

(See Table 1, Page 8, for explanation of symbols)

Fig.5. COMPARISON OF MEASURED COMPLIANCE VALUES WITH KANNINEN EXPRESSION[10]

III. RESULTS AND DISCUSSION

Examples of the plastic zones observed on the surface and in the interior on the specimen midsection are presented in Figures 6-9. The general appearances of the zones are in the main, similar to those displayed by zones in tensile loaded plates.[4] Values of ρ, the furthest extent of the zone measured normal to the plane of the slit, are about 25% larger in the interior of the DCB specimens (on the plate midsection) than on the surface, a feature also displayed by the tensile loaded plates[4]. Table 1 shows that this is not a question of specimen alignment since a given zone extends about the same amount on opposite surfaces of the same specimen.

Values of β, the specimen thickness to zone size index*, are in the range $1.25 \geq \beta \geq 0.32$ for the current series of experiments. The β-values are for the most part larger than $\beta = 0.4$, which is a suggested upper limit for achieving plane strain conditions in tensile loaded plates.[2] However, since the ρ-values for the DCB are about half the value for tensile loaded plates, the limiting value of β could also be larger in this case. In fact, Wessel's results for HP-9-4-25 and A-302B show no significant departures from the plane strain toughness vlaue below $\beta \approx 0.7$ which corresponds to the limit $\frac{K}{\sigma_Y} \leq 0.55\sqrt{\text{in.}}$ for plane strain in 0.5 in.-thick specimens. On this basis, the DCB zones corresponding to $\frac{K}{\sigma_Y} = 0.6\sqrt{\text{in.}}$, and $0.7\sqrt{\text{in.}}$ still represent a reasonably close approximation of plane strain conditions. The zone obtained by loading to $\frac{K}{\sigma_Y} = 0.4\sqrt{\text{in.}}$ probably deviated more from that which would be expected for a crack because its size is only twice the slit root radius.

---

* $\beta = \frac{1}{t}\left(\frac{K}{\sigma_Y}\right)^2$, where t is the specimen thickness, K the stress intensity, and σ_Y yield stress.

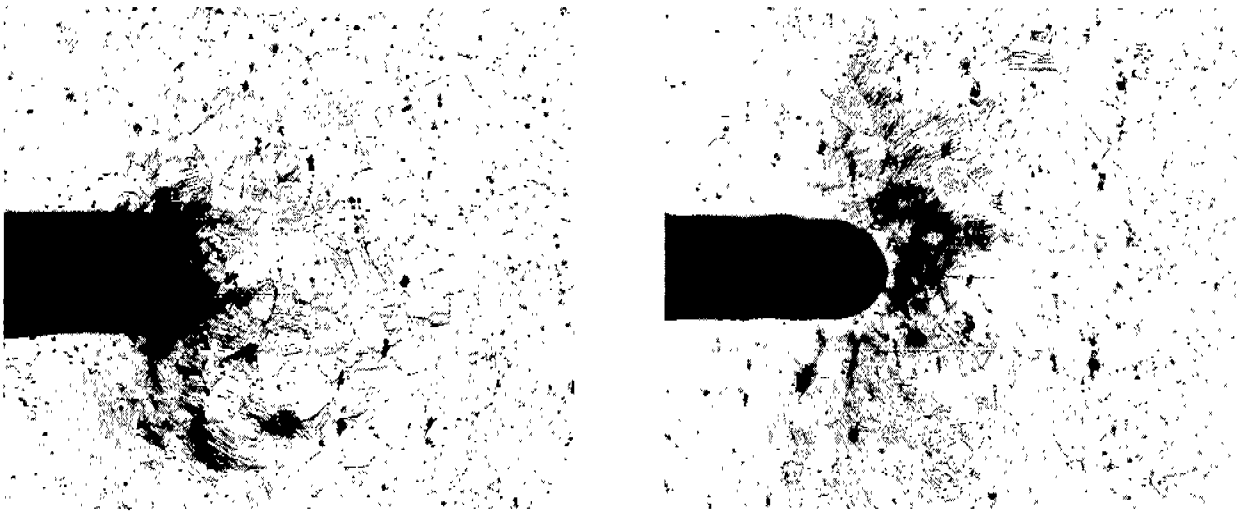

(a) surface (b) midsection

Fig.6. PLASTIC ZONE OF SPECIMEN 3P-16 LOADED TO $\frac{K}{\sigma_Y} = 0.6\ \sqrt{in.}$: (a) Specimen Surface and (b) Midsection

TABLE 1. SUMMARY OF RESULTS

TABLE 1. SUMMARY OF RESULTS

SPECIMEN	LOAD (lbs)	SLIT LENGTH (in.)	$K^{\dagger}$ ksi($\sqrt{in.}$)	$\frac{K^{\dagger}}{\sigma_Y}$ ($\sqrt{in.}$)	PLASTIC ZONE SIZE, ρ (in.) surface	midsection	opposite surface
A-3	628	3.30	49†††	0.75	-	~ 0.16	-
A-4	535	2.50	33	0.5	-	0.042	-
3P-16	2300	1.80	31	0.59	0.040	0.043	-
3P-19	2720	1.80	37	0.69	0.058	0.075	-
3P-23	1740	1.50	20	0.38	<0.010	0.009	<0.010
	2500	1.60	31	0.57	0.040	0.042	0.037
	2780	1.75	38	0.70	0.053	0.069	0.050
	2960	1.95	45	0.84	0.065	0.108	0.075
	2000	2.25	40	0.75	0.051	0.072	0.063

† $K = 2\sqrt{3}\ \frac{P}{\lambda t H^{3/2}} \left[\lambda a \left(\frac{\sinh^2 \lambda c + \sin^2 \lambda c}{\sinh^2 \lambda c - \sin^2 \lambda c} \right) + \left(\frac{\sinh \lambda c \cosh \lambda c - \sin \lambda c \cos \lambda c}{\sinh^2 \lambda c - \sin^2 \lambda c} \right) \right]$

†† Series A, σ_Y = 65.0 ksi

Series P, σ_Y = 53.5 ksi

††† Apparent

a - slit length
H - (height of arm) = 1.25 in.
t - (thickness) = 0.5 in.
P - (load)
I - (moment of inertia) = $\frac{tH^3}{12}$
c - (width of web) = 3.6 - a for Series P
λ - $(6)^{1/4}/H$

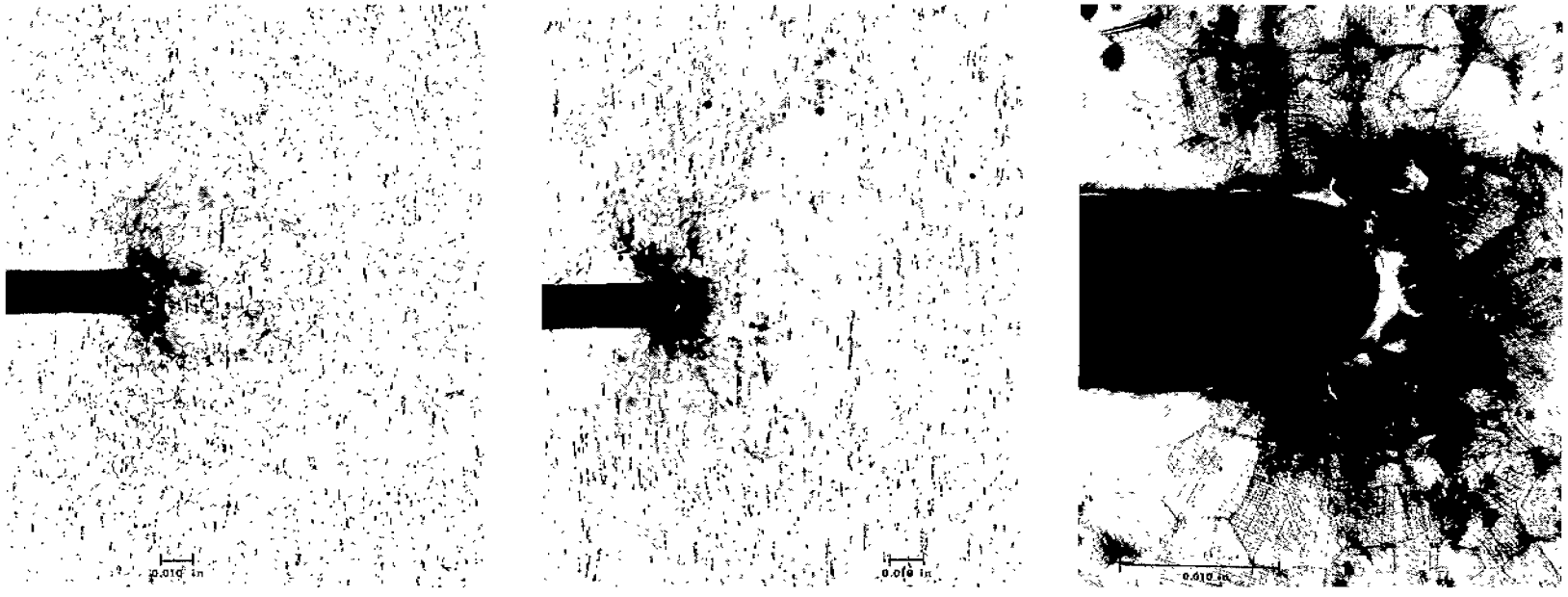

(a) Surface (b) Midsection (c) Midsection

Fig.7. PLASTIC ZONE OF SPECIMEN 3P-19 LOADED TO $\frac{K}{\sigma_Y} = 0.7\ \sqrt{in.}$:

(a) Specimen Surface, (b) Midsection, and (c) Close-up Midsection

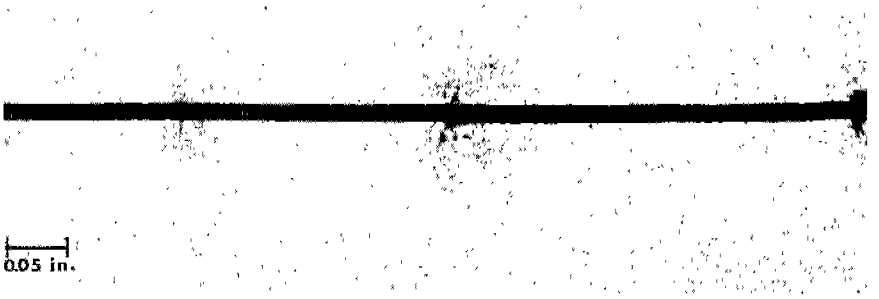

(a) Surface

$\frac{K}{\sigma_Y}$ = 0.38 $\sqrt{in.}$ 0.57 0.70 0.84 0.75

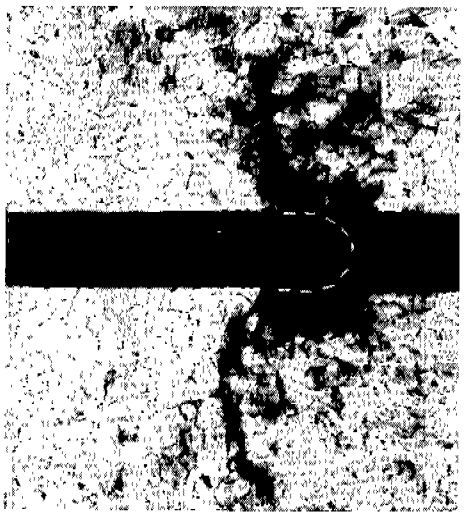

(b) Midsection, $\frac{K}{\sigma_Y} = 0.8\sqrt{in.}$

The dashed line shows the approximate position of the slit tip when the specimen was loaded. The slit was subsequently extended from left to right.

Fig.8. PLASTIC ZONES OF SPECIMEN 3P-23. A NUMBER OF ZONES WERE PRODUCED BY EXTENDING THE SLIT OUT OF RANGE OF THE ZONE BEFORE RELOADING TO A DIFFERENT STRESS INTENSITY LEVEL.

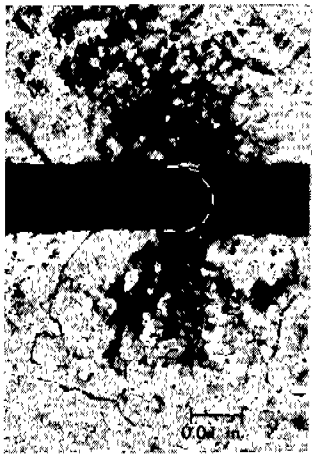

(a)

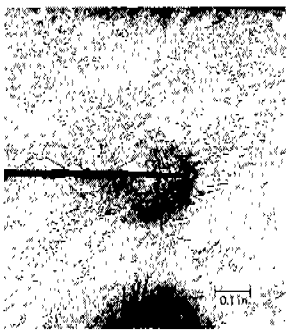

(b)

$\frac{K}{\sigma_Y}$ = 0.5 $\sqrt{in.}$

$\frac{K}{\sigma_Y}$ (apparent) = 0.75 $\sqrt{in.}$

Fig.9. PLASTIC ZONES DISPLAYED BY SERIES A SPECIMENS ON THE PLATE MIDSECTION. THE DASHED LINE IN (a) SHOWS THE APPROXIMATE POSITION OF THE SLIT TIP WHEN THE SPECIMEN WAS LOADED. THE SLIT WAS SUBSEQUENTLY EXTENDED FROM LEFT TO RIGHT.

As shown in Figure 1, the ρ-values for the DCB specimens are consistent with Clark's findings and are about 1/2 as large at comparable K-levels as the values derived from edge and center notched plates loaded in tension. In the range $0.4\ \sqrt{\text{in.}} < \frac{K}{\sigma_Y} < 0.7\ \sqrt{\text{in.}}$, the stress intensity dependence of ρ can be expressed approximately:

$$\rho \approx A \left(\frac{K}{\sigma_Y}\right)^2 \tag{1}$$

where*:

$A = 0.13$ - Etched, Series-P DCB Specimens $\frac{H}{W} = 0.35$

$A = 0.10$ - Wilson calculation for DCB specimen, $\frac{H}{W} = 0.5, \frac{a}{W} = 0.5$ and $\frac{K}{\sigma_Y\sqrt{2a}} = 0.45$

$A = 0.25$ - Etched center- and edge-notched plates in uniaxial tension[4]

$A = 0.22$ - Wilson calculation for center notched infinite plate in uniaxial tension, $\frac{K}{\sigma_Y\sqrt{2a}} = 0.45$

The ρ-values for specimens 3P-23 ($\frac{K}{\sigma_Y} = 0.8\ \sqrt{\text{in.}}$), A-4 and A-3 deviate noticeably from Equation (1), and this may be connected with the transition in zone character which is discussed in the next paragraph. Consistent with Wilson's[5] calculations, values of ℓ, the extent of the zone directly in front of the slit, are comparable to those for slits in the tensile loaded plates. As a result, the ratio $\frac{\ell}{\rho} \approx 0.2$ (for $\frac{K}{\sigma_Y} = 0.6\text{-}0.7\ \sqrt{\text{in.}}$) is about twice as large in the DCB specimens.

Figure 2 compares the outline of the zone shown in Figure 8b, $\frac{K}{\sigma_Y} = 0.8\ \sqrt{\text{in.}}$ with calculated enclaves involving nearly the same stress level and bracketing $\frac{H}{W}$ - ratios. The agreement is reasonably good considering the many imponderables: the effects of plastic straining within the zone, strain hardening, and possible departures from plane strain conditions, etc. Note that the etched zone does lean back slightly, but not as much as might be expected from a linear interpolation between the two calculated zones. Comparisons among Figures 6b, 7b, 8b, and 9 support Wilson's result, namely that the zones lean further back as the stress level is increased and as the beam height is reduced. It is also apparent from Figure 9b, that the zone finally arches over completely, thereby forming the plastic zone characteristic of a partially yielded cantilever beam.

The process of tilting back and arching over can be regarded as a transition from a crack to a beam zone, and this is likely to invalidate calculated K-values. The two zones reproduced in Figures 8b and 9a both show a small amount of

---

* a is the crack length, H the beam height, W the beam length, K the stress intensity and σ_Y the yield stress.

backward tilt, and are in a comparable, early stage of the transition. The results for these two specimens suggest a correlation between the onset of tilting (and attending deviations from calculated K-values) and the zone size to beam height ratio $\frac{\rho}{H} \approx 0.09$:

TABLE 2. ONSET OF THE CRACK-TO-BEAM-ZONE TRANSITION

Specimen	H, in.	$\frac{K}{\sigma_Y}$, $\sqrt{\text{in.}}$	ρ	$\frac{\rho}{H}$
A-4	0.5	0.5	0.042	0.085
3P-23	1.25	0.8	0.108	0.088

This ratio can be translated into a minimum specimen beam height requirement by way of Equation (1), where A = 0.13:

$$H \gtrsim 1.5 \left(\frac{K}{\sigma_Y}\right)^2 \tag{3}$$

It would appear from this and the earlier discussion that the DCB specimen beam height and thickness requirements for plane strain may be quite similar. This view is consistent with the proportions recommended by Wessel[2] for T-type specimens, i.e., H = 1.25t. However, it does raise a question about X-type specimens (H = 0.5t). In this case, departures in the plane strain toughness observed with increasing $\left(\frac{K}{\sigma_Y}\right)$ could arise from an inadequate beam height before the limiting thickness is exceeded. In addition, the difference between plastic zone size and shape in double-cantilever-beam vs straight tension specimens is puzzling since measured K_c values on both specimens are consistent. This suggests that the extent to which the plastic zone reaches out may not be a sensitive indicator of events at the crack tip. There is a need to examine this point as well as for more experiments involving systematic variations of thickness and beam height to establish minimum specimen size requirements.

IV. CONCLUSIONS

1. At low stress intensity levels, plastic zones in DCB specimens have the same general appearance as the zones in tensile loaded plates. The furthest extent of the DCB zones on the plate midsection is about half the values reported for tensile loaded plates about 25% larger than on the surface.

2. The DCB zones begin to tilt back and undergo a transition from a crack zone to the zone of a partially yielded cantilever beam at high stress levels when the zone size to beam height ratio $\frac{\rho}{H} \gtrsim 0.09$. This transition probably invalidates calculated K-values and places a lower limit on the specimen beam height which is tentatively estimated as $H \gtrsim 1.5 \left(\frac{K}{\sigma_Y}\right)^2$.

V. REFERENCES

1. R. G. Hoagland, "On the Use of the Double-Cantilever-Beam Specimen for Determining the Plane Strain Fracture Toughness of Metals", Trans ASME, Vol. 89, p. 525, 1967.

2. E. T. Wessel, "State of the Art of the WOL Specimen for K_{Ic} Fracture Toughness Testing", Eng. Fracture Mech., Vol. 1, p. 77, 1968.

3. W. G. Clark, Jr., "Visual Observation of the Crack Tip Plastic Zone Developed in a 3 Per Cent Si-Fe Alloys", Westinghouse Scientific Paper, 66-1D6-BTLFR-P1, September 27, 1966.

4. G. T. Hahn and A. R. Rosenfield, "Plastic Flow in the Locale on Notches and Cracks in Fe-3Si Steel Under Conditions Approaching Plane Strain", Ship Structure Committee Report-191, November, 1968.

5. W. K. Wilson, "Geometry and Loading Effects on Elastic Stresses at Crack Tips", Westinghouse Research Report 67-1D7-BTLPV-R1 Proprietary Class 3, July 3, 1967.

6. M. L. Williams, "On the Stress Distribution at the Base of a Stationary Crack," Trans ASME, Vol. 79, p. 109, 1957.

7. G. T. Hahn, A. R. Rosenfield, and M. Sarrate, "Observations of Yielding Accompanying Crack Growth", Inelastic Behavior of Solids, McGraw-Hill, New York, p. 673, 1970.

8. G. T. Hahn, M. Sarrate, and A. R. Rosenfield, "Experiments on the Nature of the Fatigue Crack Plastic Zone", Proc. A.F. Conf. Fatigue and Fracture, Miami, December, 1969; also AFML TR-67-143 Part III, January, 1970.

9. G. T. Hahn, P. N. Mincer, and A. R. Rosenfield, "The Fe-3Si Steel Etching Technique For Local Strain Measurement" (submitted to Experimental Mechanics).

10. M. F. Kanninen, "An Augmented Double Cantilever Beam Model for Investigating Unstable Crack Propagation and Arrest" (to be published).

Section 2

OBSERVATIONS OF YIELDING ACCOMPANYING CRACK GROWTH

by

G. T. Hahn, A.R. Rosenfield, and M. Sarrate

ABSTRACT

This paper deals with direct observations of the effects of stable growth and unstable brittle crack propagation on the plastic zone of a crack. The experiments involved Mode I and plane strain conditions and utilized Fe-3Si Steel as the model material. Stable growth was simulated by spark cutting slits under load. Cleavage crack propogation and arrest were obtained at $0^{o}C$ by wedge-loading the specimen. Plastic zones on the surface and in the interior were revealed by etching. The experiments show no striking differences between the monotonic and stable growth zones. Unlike slow growth, the propagating cleavage crack generates virtually no deformation at its tip. Instead, the deformation is associated almost exclusively with unbroken sections or ligaments left behind by the main crack front.

OBSERVATIONS OF YIELDING ACCOMPANYING CRACK GROWTH

I. INTRODUCTION

A quantitative description of the plastic zones at the tip of a crack is essential for understanding fracture. Progress is being made[1-4], but a complete analysis of the zone of the "classical" crack (stationary, virgin, and monotonically loaded) is still not in hand. In the meantime, approximate solutions have been derived from simplified models, such as those of McClintock[5], Dugdale[6] and Bilby and coworkers[7,8]. These are frequently inspired by experimental observations and have proven extremely useful. Real fractures tend to have more complicated histories than the "classical" crack. They can involve stable growth during loading, cyclic loads and fatigue growth, or unstable propagation accompanied by extraordinary strain rates and dynamic effects. These problems are even more likely to benefit from analytical shortcuts based on experiments.

With this in mind, we have made direct observations of the zones attending cracks in steel foil (plane stress). It was found that the zones produced by a stationary and slowly growing crack under monotonic loading are similar[9], but differ from the cyclic growth zone[10] and the zone attending an unstable shear crack.[9,11] The effect of crack growth was also studied in Fe-3Si Steel, where zones were revealed by etching[12]. There, crack growth was simulated in a controlled way by spark-cutting slits into specimens under load (at constant stress intensity). Under conditions approaching plane stress, the zone was wider than the zone produced by conventional loading and unloading without crack growth. Experiments were not successful under plane strain because cleavage cracks were initiated at room temperature during the spark-cutting operation.

Accordingly, the Fe-3Si experiments have now been successfully repeated at a slightly elevated temperature (100°C) which avoids cleavage. The work was also extended to cyclic loading, and to unstable cleavage crack propagation and arrest at 0°C. This paper presents direct observations of the plastic zones attending the various kinds of crack growth, both on the surface and in the interior of the metal and compares the results with the stationary, monotonic zones reported in Section 1.

II. EXPERIMENTAL PROCEDURES

Plastic zones were observed on the surfaces and on the midsections of 1/2-in.-thick Fe-3Si* Steel plates. Descriptions of the material, the etching procedure and the plastic zones produced by virgin cracks and sharp slits in tensile loaded plates are given in Reference 13. The present studies also employed the DCB (double cantilever beam) specimen as described in Section I. The experiments were conducted at 100°C (σ_Y = 54,000 psi**) in order to avoid the intrusion of cleavage, and in one case at 0°C (σ_Y = 68,000 psi) to produce a history

---

* Nominal composition: Si-3.4%, C-0.02%, remainder Fe.

** σ_Y is the yield stress.

of cleavage initiation, unstable propagation and arrest. Tensile properties of the steel at these two temperatures are shown in Figure 1. Since the 1/2-in. thickness of the DCB specimens exceeded the plastic zone size (the dimension ρ in Figure 2 by more than a factor of six, the tests approximate plane strain conditions.

The following procedures were devised to simulate different types of cracks under conditions that are comparable. The DCB specimens were mounted in a small, horizontal testing machine, immersed in kerosene and positioned directly below the cutting head of a standard spark-machining unit. The spark unit was set up to cut slits* into the test specimens with 0.005 in.-dia. copper wire at the rate $\sim$ 0.004 in. per minute. This arrangement permitted slits to be cut-in with the specimen under load in kerosene** with the temperature maintained at 100°C. DCB specimens with a pre-cut slit were loaded to some of the K-levels used in Section 1. The slit was then cut-in an additional $\sim$ 0.1 in. by spark machining under load, with the load programmed to maintain the K-level constant, and then the load was slowly removed. This experiment simulates the slow, stable growth of a crack at a constant stress intensity level.

The possibility that the results of these experiments were affected by strain aging at 100°C was examined. A Fe-3Si tensile bar was strained 1.5% at 100°C, unloaded, and then aged 10 minutes at 100°C before continuing the test at 100°C. Since this strain aging treatment only increased the flow strength about 4%, significant complications from strain aging are discounted. Two other problems are recognized. First, the interpretation of the monotonic and stable growth zones are to some extent, complicated by the superposition of the deformations attending the loading and unloading portions of the cycle. Secondly, the spark-cutting operation does remove some material (on either side of the slit center line) that is ordinarily present during actual crack growth. Although these effects are not likely to be overriding here, they could be minimized, in the first case, by aging the specimens under load (making the etch transparent to the deformation generated by unloading) and in the second case, by carrying out the cutting-in experiments in larger specimens and at a higher stress intensity level (making the slit volume a smaller fraction of the zone).

Unstable cleavage crack propagation and arrest were obtained in a DCB specimen with a pre-cut slit of length, a = 1 in. In this case the specimen was loaded at 0°C by forcing a wedge between two pins on either side of the slit. This was accomplished with the compression fixture of an ordinary testing machine as shown in Figure 3. The wedge was driven in slowly until an unstable cleavage fracture initiated. Propagation for a distance of 1.5 in. and arrest followed immediately, and probably so quickly, that these events occurred with little further wedge motion. Under these conditions, the crack propagates into a diminishing stress field. (See Section 3 for a fuller description of the variation of stress intensity, K, with crack length.)

---

* The cut slit was 0.010 in. wide with $\sim$ 0.005 in.-root radius. Since spark machining does not produce plastic flow on this scale, the tip of the slit was essentially strain-free.

** Since cleavage cracks are also initiated at room temperature when the spark cutting is performed in C Cl_4, we conclude that the earlier difficulties with cleavage were probably not related to hydrogen embrittlement, but simply to the high transition temperature of Fe-3Si.

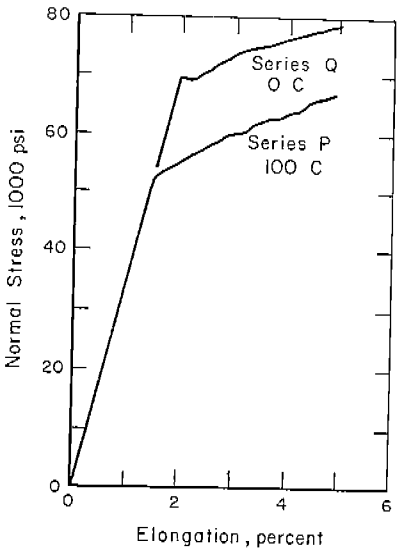

Fig.1. STRESS-STRAIN CHARACTERISTICS OF THE Fe-3Si STEEL AT 0°C COMPARED WITH 100°C

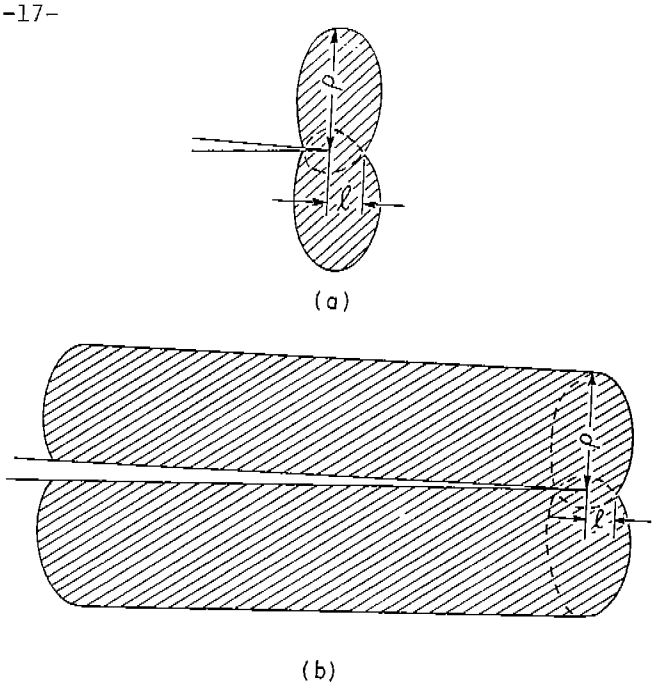

Fig.2. SCHEMATIC DRAWINGS OF THE PLASTIC ZONE PRODUCED BY: (a) STATIONARY CRACK AND (b) GROWING CRACK

Fig.3. ARRANGEMENT USED IN WEDGE LOADING OF A DOUBLE-CANTILEVER-BEAM (DCB) SPECIMEN

III. RESULTS

Plastic zones produced by the monotonic loading procedure* were shown in Figures 6 and 7 of Section 1. These are to be compared with the zones produced by cutting-in under load, the procedure simulating stable crack growth as shown in Figures 4 and 5. Here the etched sections reveal both the deformation left behind by the growing slit and the new deformation generated at the tip (as shown schematically in Figure 2). Comparisons with the zones in Section 1, Figures 6 and 7, which involve the same peak stress intensity levels, do not reveal any significant differences between the monotonic and the stable growth zone: both the sizes of the zones (see Table 1) and the near tip strain distribution (compare Figure 5c with Section 1, Figure 7c) are virtually the same. The correspondence of both zone size and strain distribution is in accord with simplified elastic-plastic analyses which predict a direct relation between zone size and the COD which, in turn, is closely related to the strain distribution.**

A common feature of all these zones is the difference in the appearance of the zones on the plate surface and plate midsection. The forward extent of the zones (the Dimension ℓ in Figure 2) was greater on the surface, while the furthest extent (the Dimension ρ roughly normal to the crack plane in Figure 2) was about 25% greater in the interior. These relations apply to both the front and back plate surface and are not connected with eccentricities in loading.

The plastic zones attending cleavage initiation, propagation and arrest are shown in Figures 6 and 7. The large plastic zone existing near the original slit tip (Figure 6a) is consistent with load required to initiate cleavage fracture at this temperature. Figures 6b, 6c, and 7 show clearly that the zone attending initiation is left behind by the propagating crack. Unlike the slow stable growth, unstable cleavage propagation proceeds with virtually no evidence of a continuous strip of plastic deformation on either side of the crack. Deformation is observed and this is associated almost exclusively with unbroken sections or ligaments left behind by the main crack front.*** More deformation is evident at the point of arrest (see Figure 6c). The unusual distribution on the surface is, in this case, related to the fact that the crack extended farther in the center of the plate (tunneled). All or part of the deformation attending arrest may have been produced by the elastic energy stored in the testing system and released after the crack had already stopped, and may be unrelated to the factors causing arrest.

IV. DISCUSSION

While the present work shows no differences between the monotonic and the stable growth zone for Mode I and plane strain, a question remains because the observations involved unloading. Similar experiments have revealed that the zones

---

* Note that this represents one cycle of loading and unloading.

** $\text{COD} = \left(\frac{8}{\pi}\frac{\sigma_Y}{E}\right)\rho$, where ρ is the zone size, E is the elastic modulus and σ_Y is the yield stress[8]. This relation is valid at relatively low nominal stress levels σ: $\sigma < 0.7\,\sigma_Y$.

*** Metallographic studies involving repeated sectioning of the sample reveal that all the cracked segments are connected.

TABLE 1. SUMMARY OF RESULTS

SPECIMEN	LOAD (lbs)	SLIT LENGTH (in)	$K^{\dagger}$ (Ksi$\sqrt{in}$)	$\frac{K^{\dagger}}{\sigma_Y}$ ($\sqrt{in}$)	PLASTIC ZONE SIZE, ρ (in) surface	midsection
Simulation of Monotonic Loading (slit at 100°C)						
3P-16	2300	1.80	32	0.6	0.040	0.043
3P-19	2720	1.80	38	0.7	0.058	0.075
Simulation of Stable Growth (slit at 100° C)						
3P-17	2300-2220	1.80-1.90	32.2	0.6	0.035	0.048
3P-18	2720-2640	1.80-1.88	38.0	0.7	0.055	0.074
Cleavage Initiation, Propagation and Arrest at 0° C						
3Q-16	-	$1.0^{(a)}$ - $2.5^{(b)}$	$50^{(a)}$-$17^{(b)}$	$0.73^{(a)}$-$0.25^{(b)}$	-	$0.080^{(a)}/0.008^{(b)}$

† $K = P\left[\frac{3(a + a_o)^2 + h^2}{3b(1 - \nu^2)\, I}\right]^{1/2}$

†† σ_Y(100 C, Series P) = 54 Ksi

σ_Y(0° C, Series Q = 68 Ksi

a - slit length
a_o - (0.6h) = 0.75 in
h - (height of arm) = 1.25 in
b - (thickness) = 0.5 in
ν - (Poissons ratio) = 1/3
P - (load)
I - (moment of inertia) = $\frac{bh^3}{12}$

(a) Corresponding with cleavage initiation

(b) Corresponding with cleavage arrest

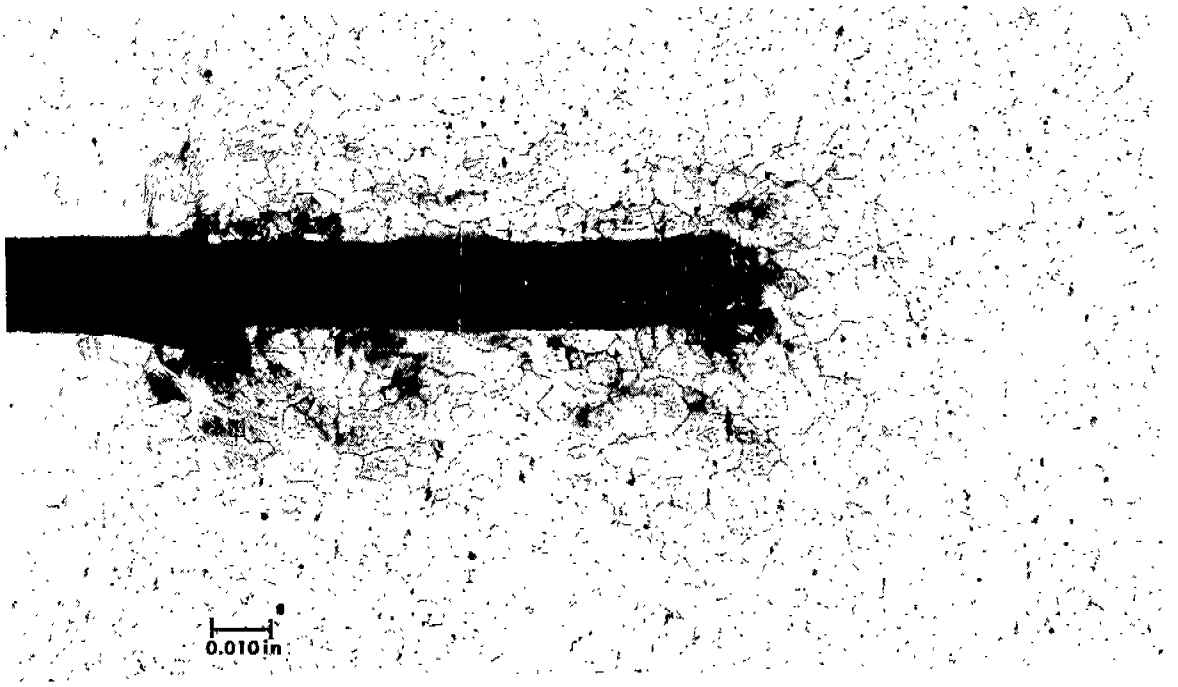

(a) surface

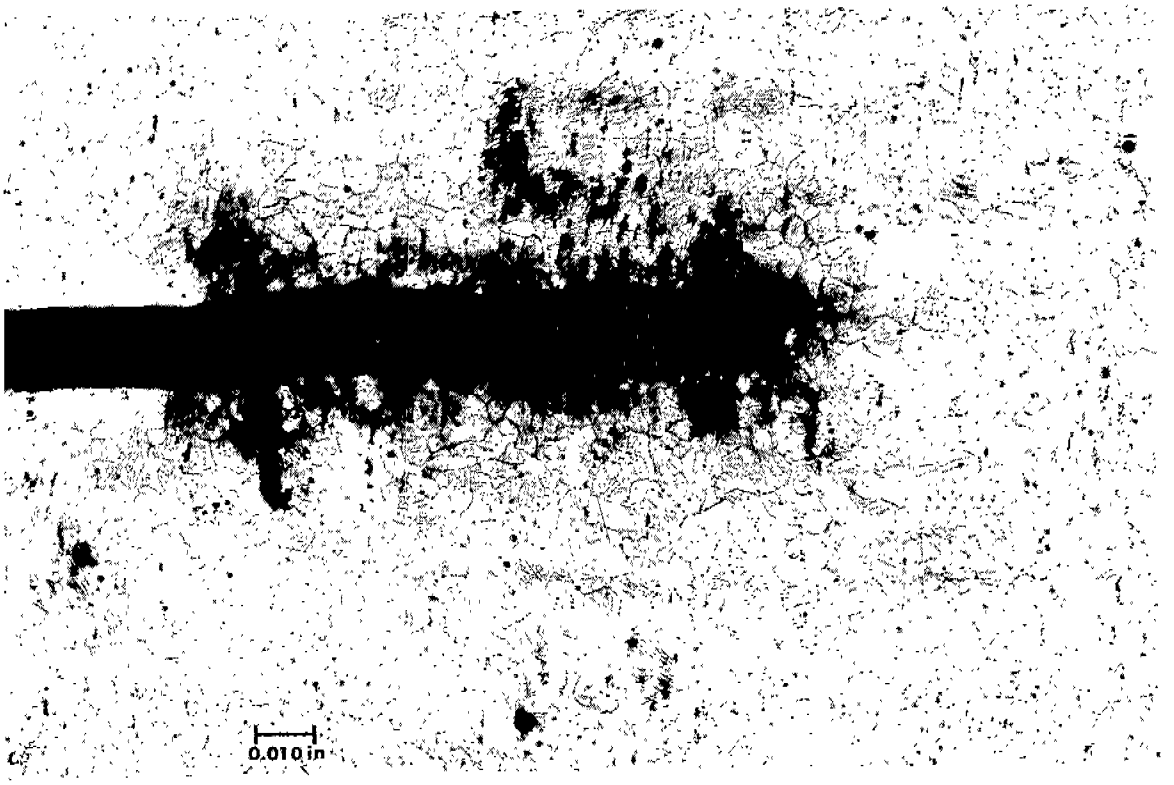

(b) midsection

Fig.4. PLASTIC ZONE FOR SPECIMEN 3P-17 FOR SLIT CUT IN UNDER LOAD CORRESPONDING TO: $\frac{K}{\sigma_Y} = 0.6\sqrt{in.}$: (a) Specimen Surface and (b) Midsection.

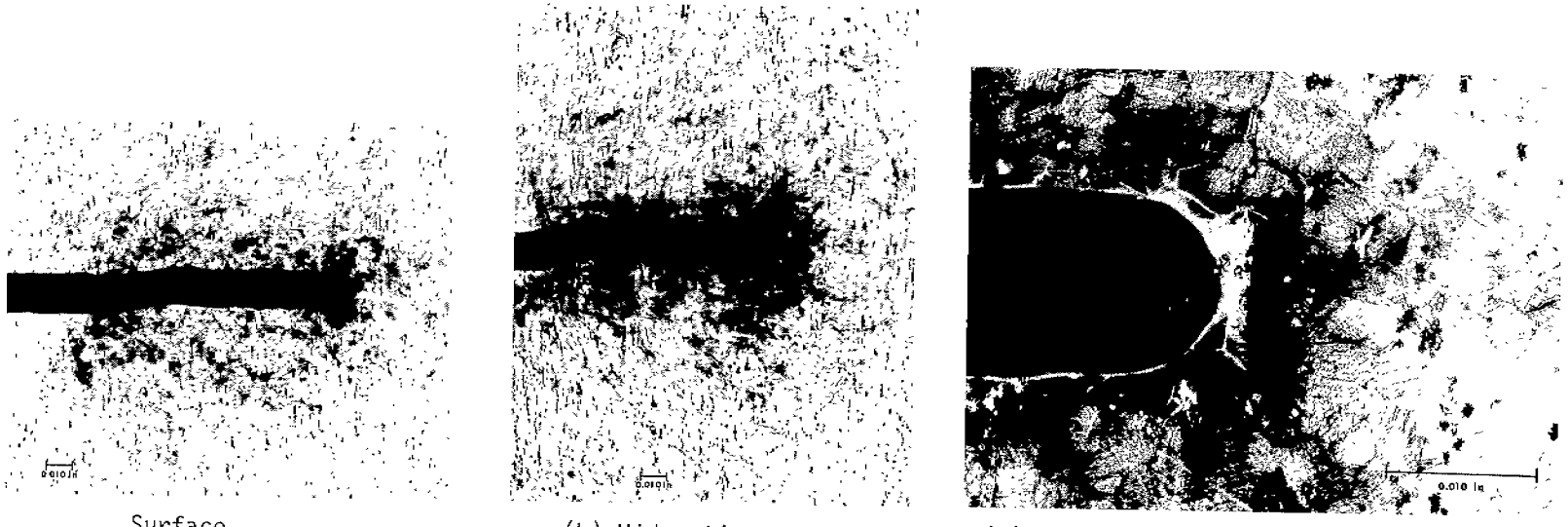

Surface (b) Midsection (c) Midsection, Close-Up of Slit Tip

Fig.5. PLASTIC ZONE OF SPECIMEN 3P-18 FOR SLIT CUT IN UNDER LOAD CORRESPONDING TO $\frac{K}{\sigma_Y} = 0.7 \sqrt{in.}$

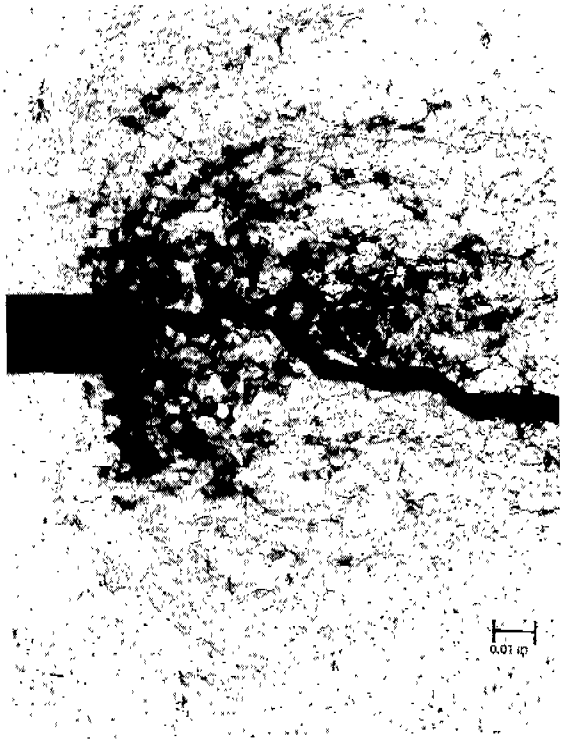

Fig.6. PLASTIC DEFORMATION ASSOCIATED WITH CLEAVAGE FRACTURE ON THE SURFACE OF Fe-3Si SPECIMEN 3Q-16. The photographs of the specimen surface show portions of a cleavage crack that was produced by wedge-loading the specimen at 0°C:

(a) near the slit tip where the crack initiated:

(b) propagation region ∿ 1.1 in. from slit:

(c) point of arrest ∿ 1.5 in. from slit

(a) initiation

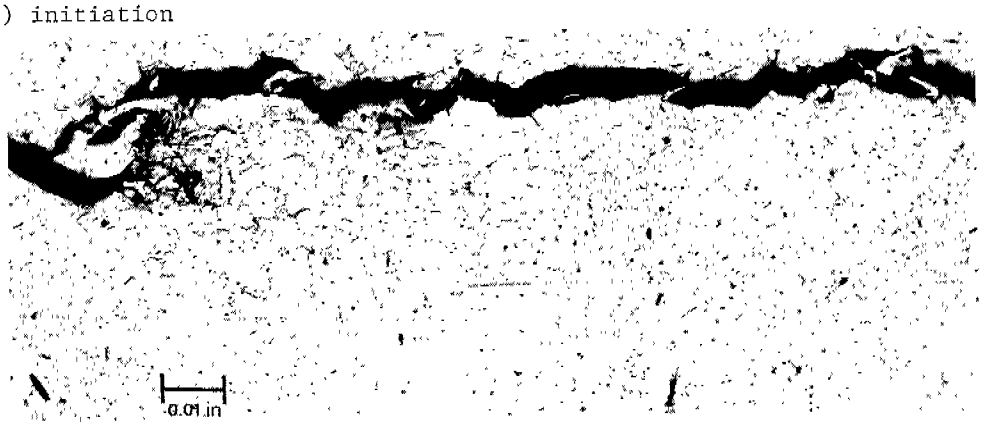

(b) propagation

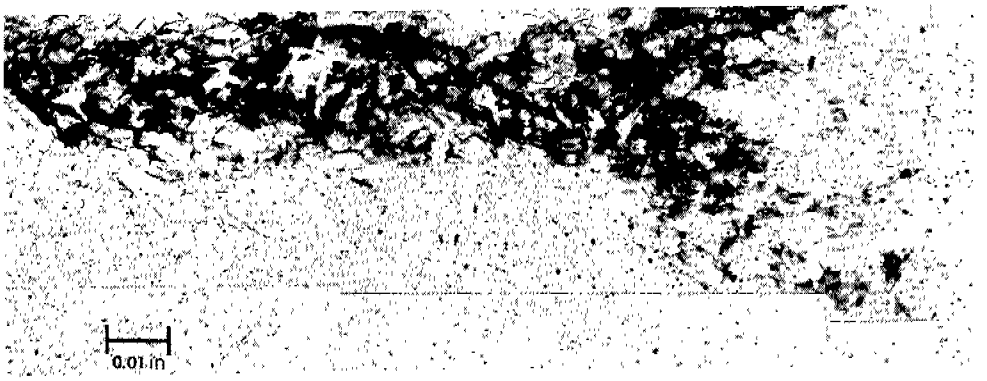

(c) arrest

Fig.7. PLASTIC DEFORMATION ASSOCIATED WITH CLEAVAGE FRACTURE ON THE PLATE MIDSECTION OF Fe-3Si SPECIMEN 3Q-16. 150X

of fatigue cracks are larger than expected[10], possibly because the yield stress is lower after a stress reversal (Bauschinger effect). With a reduced yield stress, more plastic deformation is produced during unloading and this may make it difficult to see the differences that existed before the load was removed. The problem could be overcome by aging the test specimens under load and cooling prior to unloading, a procedure that makes the unloading deformation transparent to the etchant.

The present results are in accord with observations of steel foil under load[9-11], showing that crack growth proceeds with no major changes in the plastic zone, provided the crack speed is reasonably slow. However, the zone size and presumably the crack-tip displacement do depend on the fracture mechanism, the most striking example being the marked difference between the zone attending cleavage cracking and those attending other fracture modes.

These results are in conflict with a proposal of McClintock[14,15] that the plastic zone in front of a slowly growing crack differs noticeably from that in front of a static crack. McClintock's proposal was offered as an explanation for stable crack growth and without this "history effect" another explanation is necessary. Previous experiments in this laboratory[16] have shown that stable crack growth in sheets (~0.1 in. thick) generally consists of crack advance at the midsection (tunneling) accompanied by plastic flow transverse to the sheet surface. In other materials, such as hot-worked aluminum alloys, delaminations occur parallel to the surface[17] offering another possible mechanism. In either case, stable crack growth can often be explained by the release of triaxial stresses and can be thought of as a transition from plane strain fracture towards plane stress fracture.

The extremely limited amounts of plasticity left behind by the rapidly moving cleavage crack arise from a number of sources none of which are operative in the other specimens. In the first place the nature of the cleavage process plays a role. As suggested most recently by Dvorak[18], the progress of the crack front will be highly irregular; it will extend readily through grains favorably oriented for cleavage leaving behind unbroken grains which are less favorably oriented. These unbroken grains will serve as links or ligaments, tending to hold the metal together, until they eventually fail by tearing apart. This observation is reminiscent of a model suggested by Krafft.[19] Ligament mechanism can be idealized with a modified Dugdale model consisting of a crack under load which is restrained at its tip by a discrete array of evenly spaced pinching forces. We find that the ligaments can account approximately for a factor of two reduction in the stress intensity factor, K. Another factor of two reduction in K can arise from the nature of the DCB specimen, since the stress intensity falls as the crack extends under wedge loading conditions. There is also a decrease due to dynamic effects. Measured crack speeds in steel plates[20-22] are on the order of 1/3 C (C = sonic velocity). Broberg's calculation[23] suggests that cracks moving at this speed are accompanied by a stress intensity diminution which is again on the order of 1/2.

Taken together, these three effects decrease the stress intensity factor of a rapidly moving cleavage crack in a DCB specimen by almost an order of magnitude, compared to a stationary crack. Since the plastic zone size depends on $(K/Y)^2$, it could be thus reduced by a factor of 50-100. In fact, close examination at high magnification away from the links of Figures 6 and 7 show that the zone extent is less than 1/200 of the static value. The remaining zone shrinkage can easily be accounted for by the high strain rates at the crack tip, and the corresponding yield stress elevation. Eftis and Krafft[24] estimate a crack tip strain rate of $10^7 sec^{-1}$ Unfortunately, reliable yield stress data exist only up to $10^5 sec^{-1}$, for which strain rate the yield stress of silicon iron is about 2-1/2 times its static value.[9] In any event, yield stress elevation can contribute at least as much to zone shrinkage as any of the effects which decrease K. Furthermore, it is quite likely that the stress at the tip of a running cleavage crack is on the order of the theoretical strength of the lattice.

Cleavage fracture also appears to be unique in that the zone associated with crack initiation is much larger than the zone associated with crack propagation. The reasons for this may arise from effects discussed by Griffiths and Oates.[25] They have suggested that the large energy for crack initiation represents the difficulty in raising local values of the stress and strain to sufficient levels to initiate cleavage in individual ferrite grains (these ideas are discussed further in Section 4). Based on this reasoning, one would conclude that crack extension by cleavage is a relatively inefficient process and that considerable amounts of energy are wasted in initiating cracking on the microscopic scale. Once microcracking begins, however, the energy requirements are substantially reduced and this makes it difficult to arrest a cleavage fracture.

V. REFERENCES

1. J. L. Swedlow, Int. J. Fracture Mech., Vol. 5, p. 25, 1969.

2. J. W. Hutchinson, J. Mech. Phys. Solids, Vol. 16, p. 13, 1968.

3. J. R. Rice and G. F. Rosengren, J. Mech. Phys. Solids, Vol. 16, p. 1, 1968.

4. J. R. Rice and M. A. Johnson, Inelastic Behavior of Solids, M. F. Kanninen, et al, McGraw-Hill, New York, p. 641, 1970.

5. J.A.H. Holt and F. A. McClintock, IX Int. Congress Appl. Mech., Vol. 8, p. 51, 1956.

6. D. S. Dugdale, J. Mech. Phys. Solids, Vol. 8, p. 100, 1960.

7. B. A. Bilby, A. H. Cottrell, and K. H. Swinden, Proc. Roy. Soc., Vol. A272, p. 304, 1963.

8. B. A. Bilby and K. H. Swinden, Proc. Roy. Soc., Vol. A285, p. 22, 1965.

9. G. T. Hahn, M. F. Kanninen, and A. R. Rosenfield, Fracture 1969, P. L. Pratt, et al, ed., Chapman and Hall, London, p. 58, 1969.

10. G. T. Hahn, A. R. Rosenfield, and M. Sarrate, Technical Report AFML-TR-67-143, Wright-Patterson Air Force Base, Ohio, September 30, 1969.

11. M. F. Kanninen, A. K. Mukherjee, A. R. Rosenfield, and G. T. Hahn, Mechanical Behavior of Materials under Dynamic Loads, U. S. Lindholm, ed., Springer-Verlag, New York, p. 96, 1968.

12. G. T. Hahn and A. R. Rosenfield, Int. J. Fracture Mech., Vol. 4, p. 79, 1968.

13. G. T. Hahn and A. R. Rosenfield, Report SSC-191, Ship Structure Committee, Washington, D. C., 1968.

14. F. A. McClintock, J. Appl. Mech., Vol. 25, p. 581, 1958.

15. F. A. McClintock, Proc. Roy. Soc., Vol. A 285, p. 58, 1965.

16. G. T. Hahn, A. K. Mukherjee, and A. R. Rosenfield, Eng. Fracture Mech., in press.

17. R. E. Zinkham, Trans AIME, Vol. 245, p. 1919, 1969.

18. J. Dvorak, Fracture 1969, P. L. Pratt, et al, eds., Chapman and Hall, London, p. 338, 1969.

19. J. M. Krafft, Appl. Matls. Res., Vol. 3, p. 88, 1964.

20. A. A. Wells and D. Post, Proc. Soc. Exptl. Stress Anal., Vol. 16, p. 69, 1958.

21. H. C. van Elst, Trans AIME, Vol. 230, p. 460, 1964.

22. J. M. Cragill, J. Mech. Eng. Sci., Vol. 5, p. 28, 1963.

23. K. B. Broberg, Arkiv for Fysik, Vol. 18, p. 159, 1960.

24. J. Eftis and J. M. Krafft, J. Basic Eng., Vol. 87, p. 257, 1965.

25. J. R. Griffiths and G. Oates, Fracture 1969, P. L. Pratt, et al, eds., Chapman and Hall, London, p. 229, 1969.

Section 3

MECHANISMS OF FAST FRACTURE AND ARREST IN STEELS

by

R. G. Hoagland, A. R. Rosenfield, and G. T. Hahn

ABSTRACT

The initiation and arrest of cracks in four steels having widely different yield strengths was studied as a means of characterizing the energy absorption rate during rapid propagation. The fracture tests were conducted on DCB specimens which were loaded by wedging, an arrangement which proved useful because of its inherent stiffness and because side grooves were unnecessary. Stable crack propagation in which the initiation stress intensity, K_Q, and the arrest stress intensity, K_a, were nearly equal, was observed to occur in each steel. K_Q was systematically varied by changing the root radius of the starter slot. Generally small increases in K_Q above the stable propagation level were found to produce relatively abrupt decreases in K_a to $K_a/K_Q \leq 0.4$. This behavior could be explained by appealing to a simple energy balance which provided a relation between K_a and K_Q in terms of R_d, a velocity insensitive energy absorption rate. An adequate fit to the DCB test results for all four steels could be obtained on the basis that $R_d = 2/3\ G_{Ic}$. Detailed metallographic and fractographic examinations were made which established that, at least during cleavage, the crack advances in a nonplanar fashion generating grain size unbroken regions or ligaments which remain unbroken for relatively large distances behind the crack front. From observation of deformation attending propagation in Fe-3Si, it was found that these ligaments deform and rupture during propagation, a process which can account for the overall energy of propagation. Deformation associated with the crack-tip during propagation could not be resolved. These results together with an analytic model of a crack subject to tractions, suggest that the formation of unbroken regions is the principal source of crack propagation resistance in steel.

MECHANISMS OF FAST FRACTURE AND ARREST IN STEELS

I. INTRODUCTION

Crack propagation and arrest assume importance when a structure contains isolated regions of low toughness. While such regions are likely sources of unstable cracks, they need not pose a threat to the structure. An unstable crack emerging from a "bad" region can still be arrested in the surrounding "good" (standard quality) material provided the "good" material has a sufficiently large resistance to propagation for the stress applied. The Charpy and drop weight impact tests offer a measure of crack propagation resistance. Their usefulness as inputs to design are derived from intercomparison of test results or comparison against an empirically derived scale. The Robertson[1], ESSO[2], and double tension test described by Yoshiki, et al[3] provides a combined measure of applied stress, crack length, and temperature for which arrest is possible. From this data, the stress intensity at arrest can be calculated and Yoshiki, et al show that for equivalent specimen geometries, good agreement in conditions for arrest is obtained between propagation into a temperature gradient and propagation through a uniform temperature distribution. The latter test is a "go or no-go" measurement as the test determines whether or not propagation is possible for a given set of stress and temperature conditions. A review of these techniques and the influence of the energy absorption rate of a running crack on the conditions for propagation and arrest has been written by Bluhm[4].

In several instances, crack propagation test results have been interpreted to show that the energy absorption rate, R, for a rapidly running crack is less than G_{Ic}, the crack resistance at the onset of propagation. For example, Itagaki, et al[5] obtained qualitative agreement between the ESSO and double tension test results and a prediction of energy absorption rates based on a dislocation model. For constant stress and temperature, their model predicts that plastic work expended at the crack tip decreases with increasing crack speed. This result was also inferred by Hoagland[6] based on a comparison of initiation and arrest toughness values obtained for several steels and also for an aluminum and zirconium alloy. In these tests, a double-cantilever-beam specimen was used in which initiation and arrest of crack propagation could be accomplished several times in the same specimen. The stress intensity at arrest in these materials was always lower than the initiation value and in the case of steels, arrest occurred as low as one-half the initiation level.

Confusion concerning even the qualitative aspects of crack propagation resistance still exists as opposing interpretations have been proposed for similar steels. One of the first direct measurements of the energy expended during rapid crack propagation was made by Wells[7] in which he recorded the heat input to the crack plane. His results indicate that R for a crack which is moving rapidly is greater than at the onset of propagation, although there is some uncertainty in the G_c data because of widespread yielding of his notched specimens prior to fracture. Using very thin specimens and applying the same basic technique as Wells, Weichert and Schonert[8] found the opposite behavior for steel. It is possible, however, that the differences between these two sets of results could be attributed, in part, to differences in thickness of the test specimens. Decreasing thickness will favor a transition in fracture mode from flat fracture to through-the-thickness shear and the dynamic R for these two fracture modes may respond differently to crack velocity.

TABLE 1. COMPOSITION AND YIELD STRENGTH PROPERTIES

TABLE 1. COMPOSITION AND YIELD STRENGTH PROPERTIES

Material	C	Mn	P	S	Si	Ni	Cr	Mo	Temperature (°C)	Yield Strength (ksi)
4340	0.40	0.70	0.04	0.04	0.27		0.95	0.20	22	240
									-196	310
A-517	0.15	0.80	0.008	0.013	0.26	0.86	0.48	0.42	22	109
									-135	160
									-196	178
		N	O							
Fe-3Si	0.018	0.001	65 ppm		3.5				100	55
									22	62
									0	65
									-75	95
									-196	130
Mild Steel	0.22	0.36	0.016	0.031					22	40
									-112	50
									-196	95

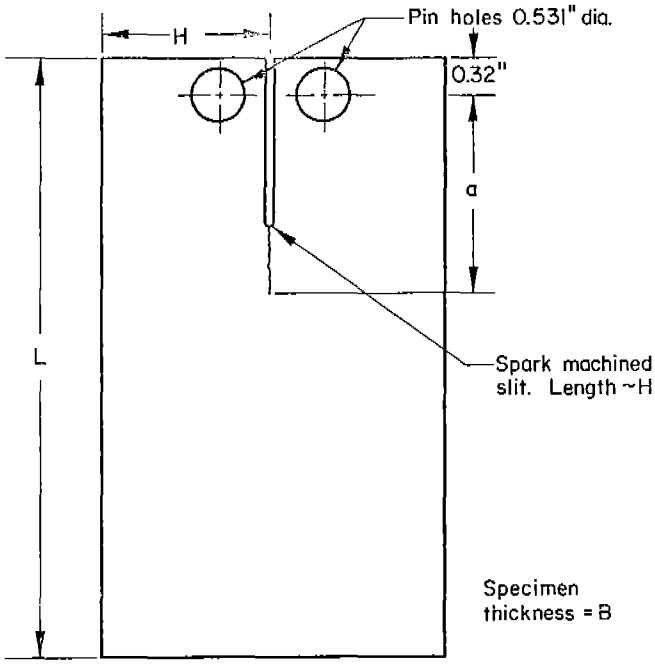

Approximate Specimen Dimensions

Material	L	H	B
4340	8.5	1.50	.500
A-517	4.0 / 8.5	1.50	.375
Fe-3Si	3.15	1.25	.500
E-Steel	4.0	1.50	.500

Fig.1. THE DCB TEST SPECIMEN. THE SPARK MACHINED SLIT FACILITATES STARTING THE CRACK. THE SLIT WIDTH IS A VARIABLE IN THE STUDY. IN THE CASE OF THE A-517 TWO SPECIMEN LENGTHS WERE EMPLOYED.

In a series of fracture toughness measurements of a mild steel in which both temperature and loading rate were varied, Eftis and Krafft[9] found that the initiation toughness, K_{Ic} of a mild steel, decreased with increasing loading rate to a minimum value determined by test temperature and then increased at still higher loading rates. From these results, they suggest that the energy absorption rate would follow the same trend as the crack velocity increased. They substantiate their results by estimating the stress intensity-crack velocity relation from wide plate test results obtained by Hall[10] and coworkers. These estimates indicate a rapid increase in stress intensity with crack speeds in the range of 3000 fps to 5000 fps. There is, however, an element of uncertainty in these estimates as they were not corrected for dynamic effects, effects which Broberg[11] shows to be important in this speed range. In addition, Dvorak[12] suggests that propagation is discontinuous due to the formation and rupture of unbroken links left behind as the crack grows. He further suggests that plastic deformation of these links is the principal energy absorbing process during propagation. On this basis, the processes of crack initiation and propagation could be different.

It is apparent that existing results are inconsistent and contradictory and that the actual dependence of R on crack speed remains poorly understood. A comparison of the initiation and arrest toughness seems to offer a useful method of studying the differences in the static and dynamic values of R. In fact, Crosley and Ripling have suggested[13] that the arrest toughness corresponds to the minimum R, and that a stress intensity less than this minimum would be incapable of sustaining propagation.

In this paper we present the results of crack propagation tests which compare initiation and arrest toughness for four steels having widely different strength levels. A DCB specimen and a relatively stiff loading arrangement were used in an attempt to minimize interactions between the loading system and specimen during propagation. Stress levels during propagation were altered systematically by varying the bluntness of the starting crack. This technique made it possible to relate the arrest toughness to an average energy absorption rate and the stress level at initiation. The presence of energy absorbing ligaments is demonstrated and a quantitative analysis of their role in propagation is developed.

II. EXPERIMENTAL PROCEDURE

Materials. Compositions and mechanical properties of the four steels used in this study are given in Table 1. The mild steel also known as project steel E was received as hot-rolled plate 1/2 in. thick. Several earlier studies of the tensile fracture and microcrack formation behavior have been conducted on identical material[14-15]. The ASTM specification A-517 is a constructional steel given the U. S. Steel designation T-1. It was supplied as quenched and tempered plate 3/8 in. thick. Two heats of silicon steel made from Armco Iron and from electrolytic iron were prepared at Battelle. The processing conditions of the silicon steel have been reported in detail in Reference 16. Finally, the 4340 steel was tested as water-quenched from 1550°F.

Wedge-Loaded DCB Tests. The double-cantilever-beam specimen configuration which was employed here is shown in Figure 1. Conventionally, this type of specimen is loaded in tension by a pin and yoke arrangement. Unless the crack plane corresponds to a plane of very low toughness, fairly deep side grooves must be machined down the length of the specimen[6] to guide the crack since the large bending stress in the arms cause the crack to veer to the side of the specimen. The use of side grooves suppresses the formation of shear lips and, although several studies have shown little or no effect of side grooves on the initiation toughness, there remains

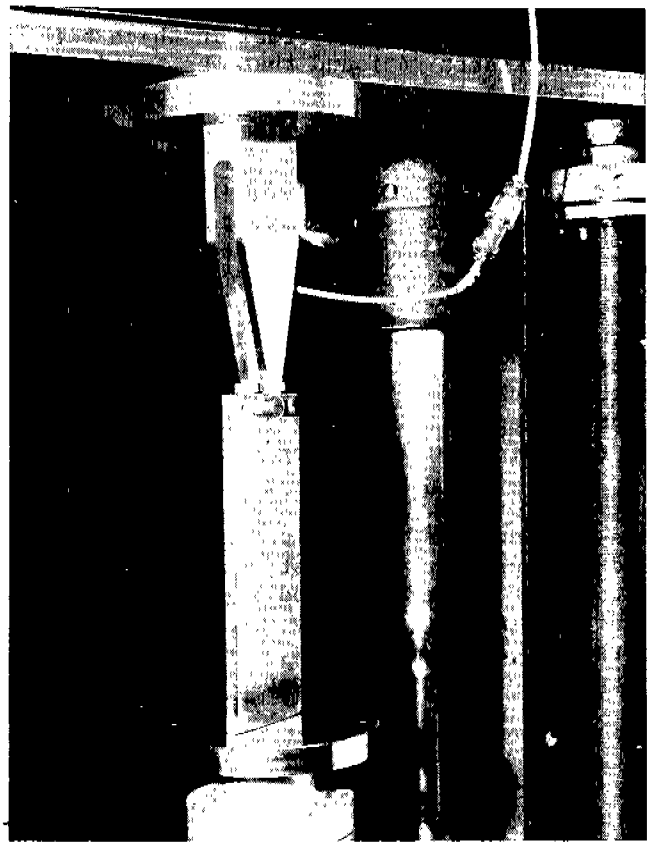

Fig.2. LOADING ARRANGEMENT. The wedge is forced between the hardened steel pins extending through the pin holes. The clip gage mounted on the specimen between the two legs of the wedge monitors displacement of the pins

a degree of uncertainty as to the effect of side grooves on the propagation behavior. To circumvent the need for side grooves in this study, the specimens were tested by forcing a wedge between the loading pins. This loading arrangement is shown in Figure 2. The force applied to the wedge by the testing machine produces a compressive stress in the specimen which reduces the tensile bending stress. As long as this longitudinal compressive stress produced by the applied force acts parallel to the crack plan , it does not affect the crack-tip singularity and therefore does not affect the applied stress intensity. For a given crack opening displacement, the stress intensity is independent of applied load. If P is the opening force on the specimen, then the load applied to the wedge, F_a, is

$$F_a = 2P \cos\theta \ (\mu \cos\theta + \sin\theta) \qquad (1)$$

where 2θ is the wedge angle and μ is the coefficient of friction between the pins and the wedge. Suppresion of the bending stress is controlled primarily by varying the wedge angle. Initially, an 11 degree wedge angle was used. For the approximate specimen dimension given in Figure 1, this wedge angle was adequate for maintaining straightforward propagation of cracks less than about 2 to 3 inches in length although longer cracks turned to the side of the specimen. A 30 degree wedge angle was used later in this study and was found to maintain the desired crack plane for cracks longer than 5 to 6 inches. It should be pointed out that even though this loading method may encourage straightforward advance of the crack at the initiation stage, several theoretical investigations have shown that the crack-tip stress field undergoes reorientation with increasing velocity to the extent that branching or at least curvature of the crack path is favored. This effect can also be suppressed by increasing the wedge angle but the required wedge angle would depend on the maximum crack speed.

An important facet of this study involves the determination of the variation in the stress intensity at crack arrest with the stress intensity at initiation. In order to increase the initiation stress intensity above the minimum sharp crack value, K_{Ic}, the specimens were provided with spark machined slots of various root diameters. These starter slots were cut to depths of not less than H, the beam height.

If the coefficient of friction is precisely known, P can be determined from F_a via Equation (1). The applied stress intensity is given by Gross and Srawley[13] as

$$K = \frac{2\sqrt{3}\,Pa}{BH^{3/2}}\left(1 + 0.7\,\frac{H}{a}\right) \tag{2}$$

In practice, very little confidence can be given to a measurement of μ since it is likely that μ varies from test to test and also with applied load (due to a slight peening of the wedge at the point of contact with the pins). Alternatively, K may be calculated from the pin displacement, y, and the crack length. If ϕ is the specimen compliance y/P, then the strain energy release rate is

$$G = \frac{y^2}{BH\,\phi^2}\,\frac{\partial \phi}{\partial a} \tag{3}$$

Since $G = K^2/E$, combining Equations (2) and (3) gives a first order differential equation for compliance as

$$\frac{d\phi}{da} = \frac{24}{EBH}\left(\frac{a}{H} + 0.7\right)^2 \tag{4}$$

which, for fixed y, integrates to

$$\phi = \frac{8}{EB}\left(\frac{a}{H} + 0.7\right)^3 + \phi_o \tag{5}$$

Approximate measurements of ϕ_o, accurate to within a factor of two, show that ϕ_o is at least two orders of magnitude less than ϕ for $a/H = 1$ and can, therefore, be neglected with little error for crack lengths longer than this. The expression for K then becomes

$$K = \frac{0.433Ey}{\sqrt{H}\left(\frac{a}{H} + 0.7\right)^2} \tag{6}$$

The actual dependence of K on crack length departs from Equation (6) for very short crack lengths and as the crack approaches the end of the specimen. Estimates[6,17] of the range of applicability of Equation (6) give

$$\frac{H}{L} < \frac{a}{L} < 1 - \frac{H}{L}$$

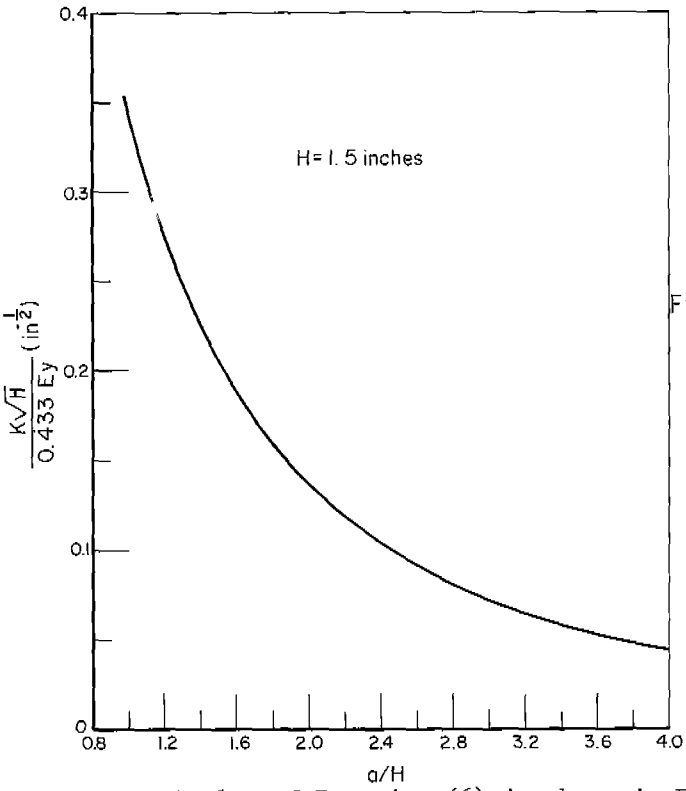

Fig.3. A PLOT OF EQUATION (6) ILLUSTRATING THE DEPENDENCE OF K ON CRACK LENGTH FOR FIXED DISPLACEMENT, y

A plot of Equation (6) is shown in Figure 3. Clearly, for a constant pin displacement, y, the applied K decreases rapidly with increasing crack length, a condition which favors crack arrest. However, truly fixed pin displacement as the crack extends could be achieved only for an infinitely stiff testing system. Relaxation of the loading system as the crack grows will produce an additional increase in y. If we let δ represent the total displacement of the system required to produce a pin displacement of y then for $d\delta/da < 0$, the specimen-load train system is inherently unstable since the stress intensity increases as the crack extends. In a detailed analysis of crack stability in various fracture mechanics specimens, Clausing[18] includes the effect of the compliance of the loading system on the condition for crack instability. From Equations (18) and (19) in Reference 18, it can be deduced that for a DCB specimen $d\delta/da$ must be positive for

$$\phi_L < 2\ \phi \tag{7}$$

where ϕ_L is the compliance of the loading system. As long as Equation (7) is satisfied, crack growth is mechanically stable.

In this study, an Instron testing machine with a 10,000 lb. load cell was used. For this loading system, the compliance (including the wedge) was found to be 5.4×10^{-6} in./lbf and, therefore, crack extension can be shown to be mechanically stable for $a/H > 1$ on the basis of Equation (7). The most mechanically compliant member of the load train is the load cell, the wedge contributing only 8% to the total compliance. The inherent stiffness of the wedge-loading technique is an advantage since increased stiffness decreases the interaction between the testing machine and the test specimen during rapid crack propagation.

Room temperature tests were conducted with the specimen loaded vertically as shown in Figure 2 while the pin displacement was recorded continuously by means of the clip gage. The gage used is similar to that described by Brown and Srawley;[19] however, the gage is attached to the specimen by conical-pivot seats mounted on both sides of the slot on the end-face of the specimen. This seating arrangement enabled a positive contact between the gage and the gage blocks thereby minimizing the effect of the shock associated with a rapid propagation event. Other arrangements proved unsatisfactory as the gage position relative to the specimen changed, or the gage was completely disloged during propagation. The gage calibration was repeatable to ± 0.0002 in. and was checked at frequent intervals during this study. While the load was not used to determine K, the load-displacement record provided a convenient means for noting the initiation and arrest conditions since a drop in the applied load signifies a propagation event. At test temperatures other than room temperature, the specimen-displacement gage assembly was either placed in a bath or, for intermediate subzero temperatures, was surrounded by a helical tube which sprayed, at controlled rates, cold N_2 gas supplied by a liquid N_2 container. After one or two propagation events, the specimen is removed from the test fixture and the crack length measured on the surface to an accuracy of ± 0.002 in. Some measurements of crack length were made on both sides of the specimen but generally this was unnecessary as the crack trace on both surfaces were very nearly equal.

III. RESULTS

DCB Test Results. A summary of the average initiation and arrest results for the four steels are compiled in Table 2. Both plane strain and non-plane strain data are referred to here as initiation toughness or K_Q. The thickness criteria in terms of the parameter $B/(K_Q/Y)^2$ which establishes the lower limit of the plane strain regime is somewhat uncertain, but is approximately in the range 1.5 to 2.5. Toughness values for which $B/(K_Q/Y)^2$ is greater than about 2.0 should, therefore, correspond to K_{Ic}.

The extent of propagation for each test condition is reflected in the difference between the initiation and arrest stress intensity K_a. It is important to note that the arrest stress intensity is determined immediately after arrest and, therefore, after the testing system and specimen have regained static equilibrium. The greater this difference, the more unstable the propagation and the farther the crack propagates before arresting. In some tests, the crack ran to the side or to the end of the specimen and, therefore, the arrest stress intensity could not be determined. In these cases, an upper limit of K_a was computed from the maximum crack length for which Equation (6) is applicable. Since propagation continued beyond this point, the actual arrest stress intensity must be less than this estimate. Examples of these propagation behaviors are shown in Figure 4. In most instances in which propagation extended from a previously arrested crack, the propagation was very nearly stable as evidenced by the fact that the initiation and arrest stress intensities are very nearly equal. In fact, for each material and test temperature, there exists a minimum stress intensity at which both initiation and propagation occur. The crack either extended slowly or in more rapid but very small increments* typically of the order of 0.020 to 0.100 in.

In the 4340, propagation was quite stable at room temperature for crack extension from both a 0.006 in.-wide slot and an arrested crack. Increasing the slot width to 0.026 in. resulted in a more than fivefold increase in the initiation threshold and loss of plane strain. In this case, the crack extended rapidly for some distance down the length of the specimen and then turned to the side of the specimen typical of a very unstable propagation in which K_a is considerably less than K_Q. The resulting crack path in this specimen is shown in Figure 4. At -196°C, the initiation threshold was elevated by a 0.006 in.-wide slot, although in this case, the condition of plane strain at the slot tip persists.

* Metallographic examination often revealed that crack extension was somewhat nonuniform along the crack front when propagation occurred in small increments.

TABLE 2. SUMMARY OF DCB TEST RESULTS

Material	Test Temperature (°C)	Slot Root Diameter (in.)	K ksi$\sqrt{in.}$ Initiation	K ksi$\sqrt{in.}$ Arrest	$\frac{B}{(K_Q/Y^2)}$
4340 As quenched	22	sharp[a]	35	32	23.7
		0.006	33	33	26.0
		0.026	82	< 50[b]	0.9
	-196	sharp	55		15.7
		0.006	81	< 29	7.4
A-517	-135	sharp	41		5.9
	-196	sharp	32	31	11.9
		0.007	42	18	6.9
		0.009	43	12	6.3
		0.025	69	16	2.5
		0.061	>117		< 0.9
Shoemaker and Rolfe notch bend[20]	-196	sharp	35 (static)	28 (dynamic)	-
Fe-3Si	100	sharp	65	~ 63	0.4
		0.026	63	~ 60	0.4
	22	sharp	28	26	2.5
		sharp	34[c]	~ 8	1.6
		0.007	28	27	2.5
		0.042	75	< 25	0.4
	0	0.010	50	12	0.9
	-75	sharp	34	33	3.5
		0.017	40	22	2.5
Project Steel E	-112	sharp	22	18	2.7
	-196	sharp	25	25	7.2
		0.007	19	23	13.1
		0.046	41	< 10	2.6

(a) Arrested crack tip.

(b) Arrest values labelled with "<" are computed assuming the crack arrested at the limits of applicability of Equation (6). The crack turned to the side or ran to the end of the specimen and, therefore, the actual K at arrest is less than this.

(c) An anomolously high initiation toughness believed to be caused by unbroken regions at the crack tip.

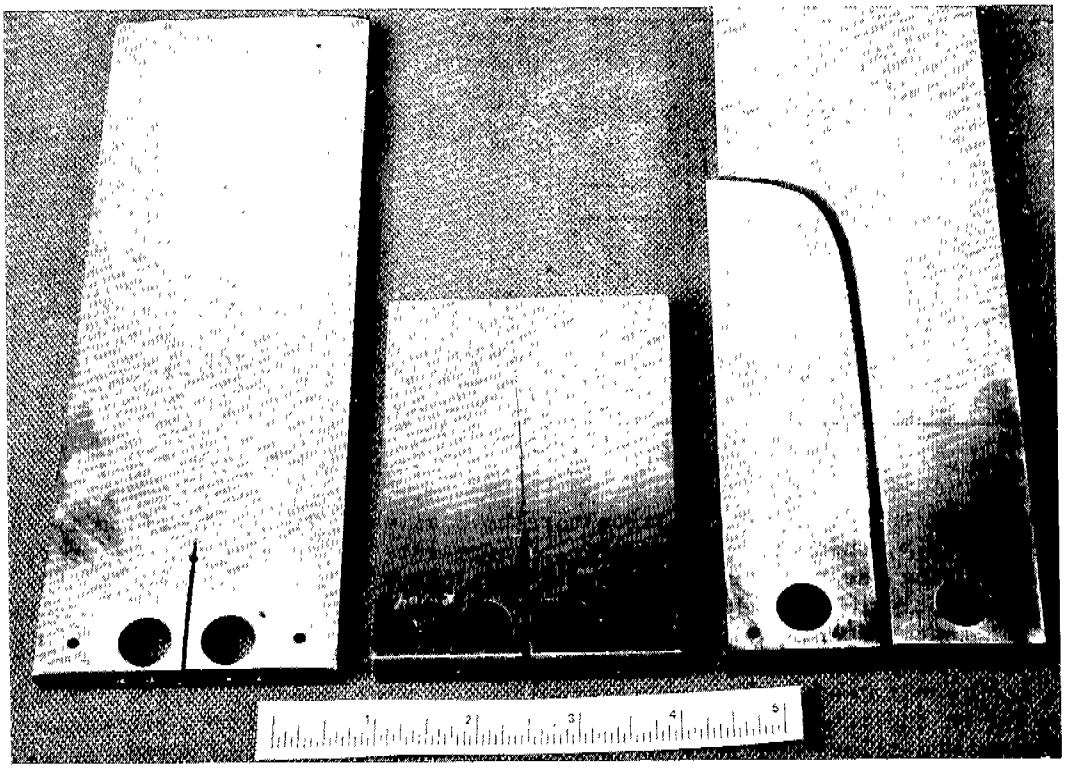

Fig.4. COMPARISON OF CRACK PROPAGATION BEHAVIOR: (a) A-517 steel in which crack extension was stable, (b) mild steel specimen in which the crack propagated in an unstable fashion from the slot tip to the end of the specimen, and (c) unstable crack in quenched 4340 which propagated from the slot tip to the side of the specimen

In the series of experiments on A-517, K_Q was progressively increased by increasing the slot width. For initiation from a sharp arrested crack, the propagation was essentially stable and the $K_Q(K_{Ic})$ and K_a are very nearly equal. For higher initiation thresholds, K_a decreases to approximately 1/2 the stable propagation value. For comparative purpose, static and dynamic (falling weight) toughness data for identical material obtained by Shoemaker and Rolfe[20] are included. Here the increased loading rate results in a 20% decrease in toughness.

In the Fe-3Si and mild steel, slot widths greater than 0.007 in. were required to elevate the initiation toughness and produce unstable propagation. However, even for a sharp crack, an anomalous increase in K_Q as, for example, occurred in Fe-3Si at 22°C results in unstable propagation and a low arrest toughness. In this particular example, the increase in the toughness from 28 ksi $\sqrt{\text{in.}}$ to 34 ksi $\sqrt{\text{in.}}$ is the result of extensive division of the arrested crack tip as described in the following section. It is also interesting to note that sharp elevation of K_Q by increasing the temperature from 22°C to 100°C did not promote unstable propagation but resulted in very slow crack extension.

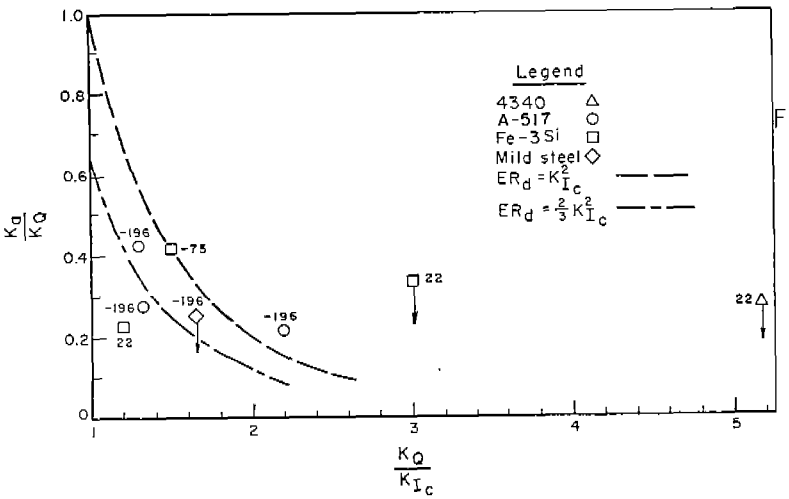

Fig.5. A COMPILATION OF THE TOUGHNESS DATA FOR THE FOUR STEELS SHOWING THE DEPENDENCE OF THE ARREST STRESS INTENSITY, K_a, ON THE INITIATION LEVEL, K_Q. Test temperatures in °C are indicated. Dashed lines are theoretical predictions based on Equation (13)

Denoting the minimum initiation threshold at which the propagation is essentially stable by K_{Ic}, then the ratio, K_Q/K_{Ic}, represents the amount of overstressing achieved by blunting the starter slot. For K_Q/K_{Ic} above unity, K_a for each of the steels falls abruptly. This behavior is summarized in Figure 5 for the four steels at each of the test temperatures where K_{Ic} was established. In this figure, the stable propagation data for these materials nearly coincides to the coordinates $K_a/K_Q = 1$, $K_a/K_{Ic} = 1$, and so have not been plotted. Also shown in Figure 5 are predictions based on the condition that the energy absorption rate during propagation, R_d, is constant and related to K_{Ic}. This point is discussed in more detail below.

Crack Propagation Behavior. In order to characterize the path of the propagation, selected specimens of each steel containing an arrested crack were sectioned and examined. The purpose of these examinations is to identify the microstructural features which may be influencing the propagation or perhaps promoting crack arrest. Scanning electron microscopy was also used to examine the fracture surfaces.

In both the Fe-3Si and mild steel, the fracture mode was found to be predominantly cleavage for the unstable as well as stable types of propagation. Typical examples of the fracture surface of the mild steel tested at -196°C are shown in Figure 6. Both areas in Figure 6 correspond to regions where crack extension occurred in small increments. Each of the nearly planar facets represents cleavage through an individual grain. At each boundary the crack plane and direction changes as the crack advances into the next grain. As a result of the random grain orientation, the crack becomes a surface extending in three dimension on a microstructural scale in contrast to the often idealized two-dimensional plane. This highly irregular crack plane seems to exert considerable influence on the propagation behavior, as discussed more fully below. A few small isolated areas which show evidence of dimples typical of ductile fracture can also be observed.

In Figure 7, the crack profile at the midthickness position of a mild steel specimen containing an arrested crack also shows that the cleavage crack path is quite discontinuous. Numerous unbroken regions or ligaments are left behind as the crack extends. In contrast to the very small size of the tensile ligaments embodied in a fracture model posed by Krafft[21], the unbroken regions here have grain size dimensions and can be found relatively large distances (~ 0.5 in.) behind the arrested crack front. These unbroken ligaments are more numerous near the crack tip which indicates that continued opening of the crack must involve rupture of the ligaments by either cleavage or a ductile tearing mechanism. It is likely that ductile rupture of the intervening ligaments is the source of the isolated dimpled regions observed on the fracture surface.

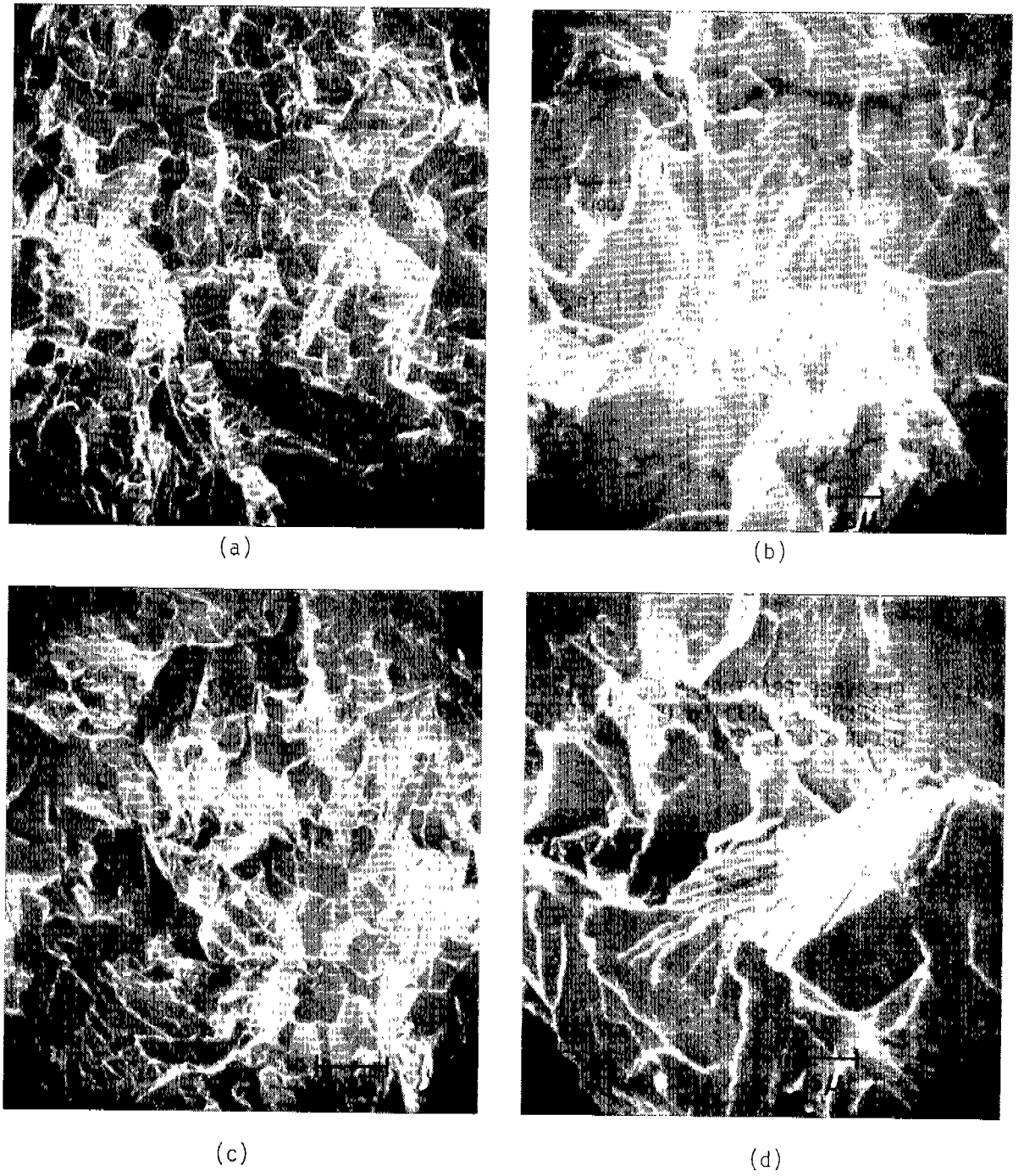

(a) (b)

(c) (d)

Fig.6. FRACTURE SURFACE OF PROJECT STEEL E FRACTURED AT -196°C. REGION OF STABLE PROPAGATION. (b) is the enlarged center portion of (a). (d) is the enlarged center portion of (c)

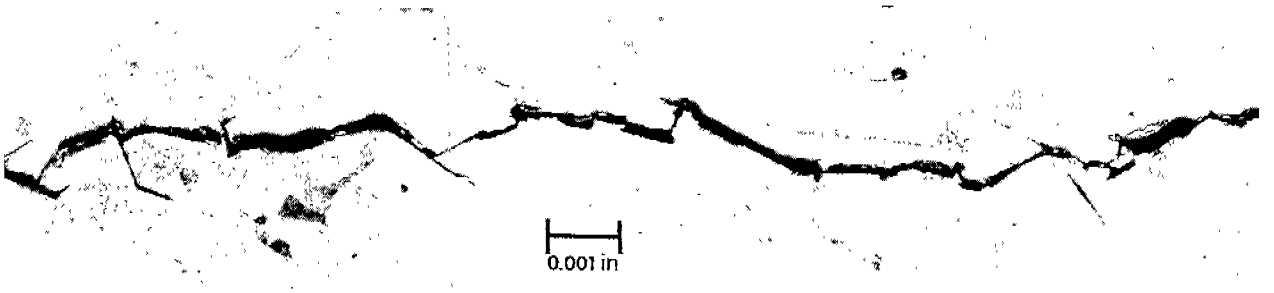

∿ 0.1 in. from final arrest

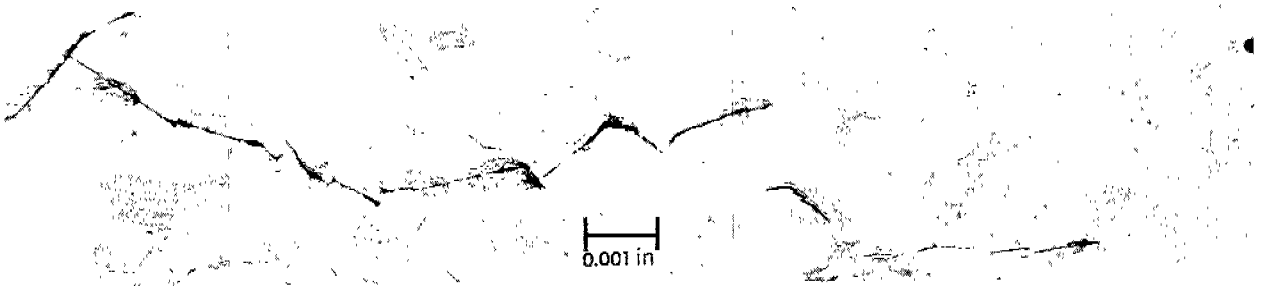

final arrest

Fig.7. CLEAVAGE FRACTURE PROFILES IN THE MILD STEEL. PHOTOGRAPHS OF THE MID-THICKNESS POSITION OF A SPECIMEN TESTED AT -196°C. CRACK EXTENSION OCCURRED BY VERY SMALL JUMPS

(a) 0.5 in. from tip

(b) arrested tip

Fig.8. CRACK PROFILES IN Fe-3Si SPECIMEN TESTED AT 0°C. THE AREAS MARKED A AND B ARE EXAMINED IN FIG.9

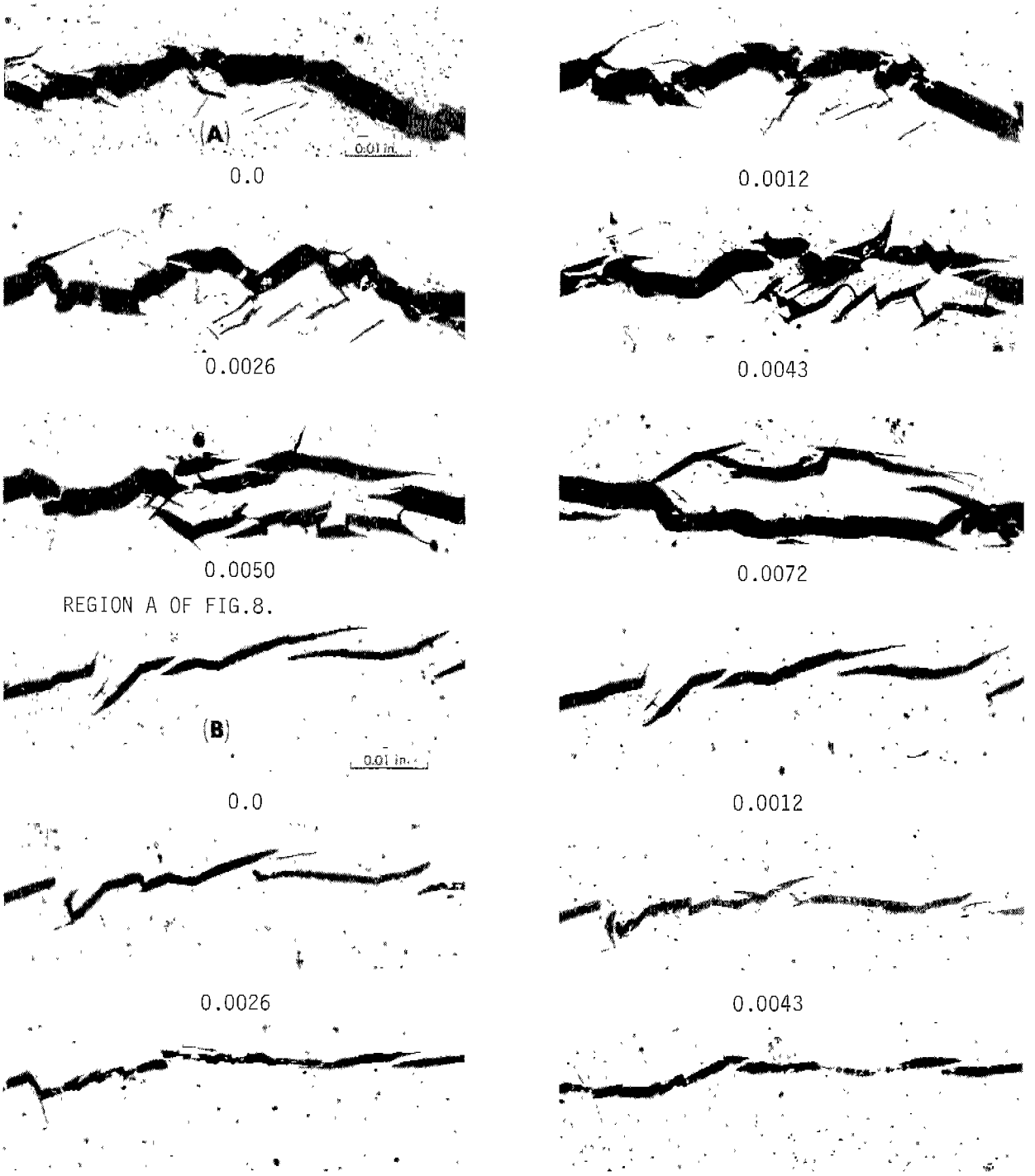

Fig.9. INTERCONNECTIONS BETWEEN MICROCRACKS REVEALED BY PROGRESSIVE SECTIONING. THE DEPTH OF EACH SECTION BELOW THE STARTING SECTION IS INDICATED

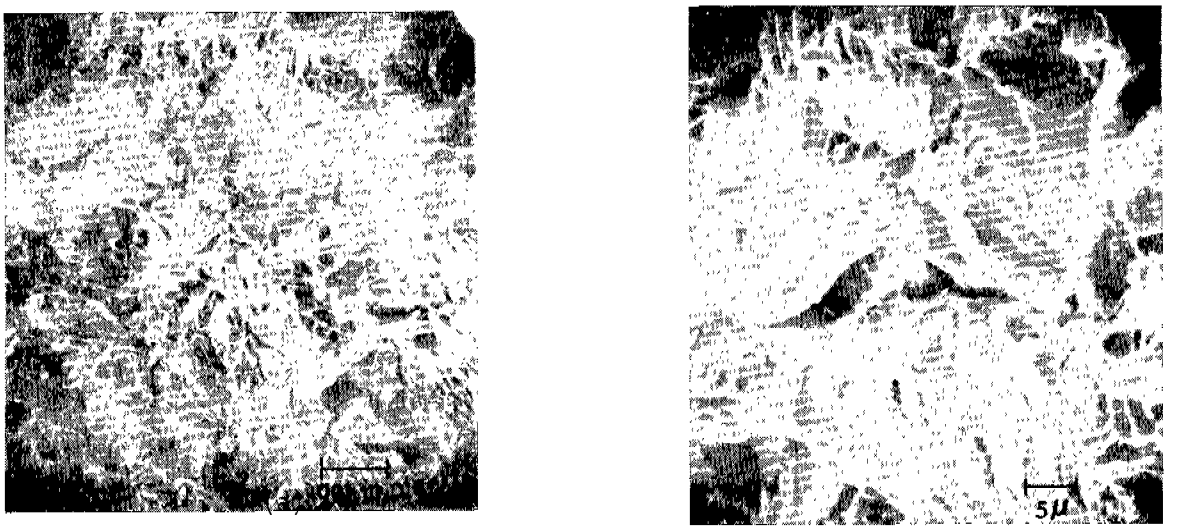

(b)

FIG.10. FRACTURE SURFACE OF A-517 TESTED AT -196°C. (b) is an enlarged portion of (a)

(a) 0.030 from crack tip (b) crack tip

FIG.11. CRACK PROFILE OF A-517 TESTED AT -196°C

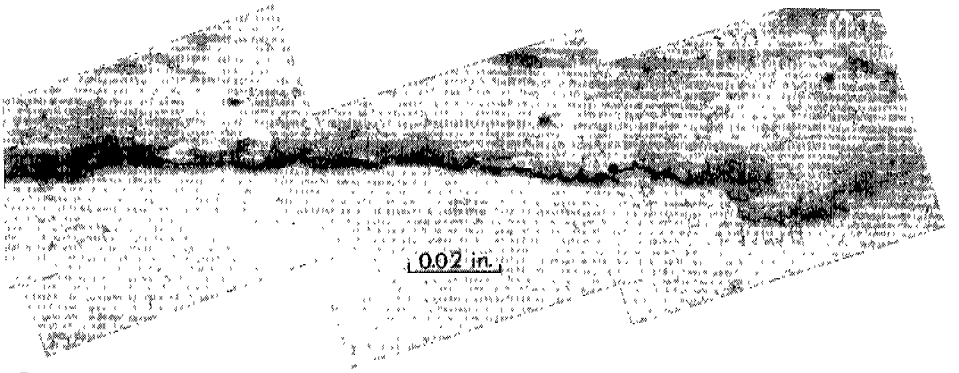

FIG.12. ARRESTED CRACK TIP IN QUENCHED 4340 AFTER UNSTABLE PROPAGATION AT -196°C

In Figure 7, it appears that several microcracks are isolated and that the ligaments perhaps form a single multiply connected network. Sections revealing the crack profile in the Fe-3Si also have the same appearance as shown in Figure 8. Here again, apparently isolated microcracks are common but become more numerous near the crack tip. By progressively sectioning in increments of about 0.002 in. (a total of twelve sections were made) it was possible to obtain a three-dimensional concept of the crack shape and better judge the degree to which the microcracks were interconnected. From the sectioning, it was found that in no instance was a microcrack observed to be completely isolated. Two examples in which apparently isolated microcracks were observed to connect to the main crack are shown in Figure 9. These results suggest at least for the Fe-3Si that the ligaments correspond to islands of unbroken material. The crack itself forms a continuous surface and truly isolated microcracks are rare. Because of the close similarity in the fracture topography with the Fe-3Si, this result should also apply to the mild steel although this material was not progressively sectioned.

In the A-517, which has a quenched and tempered microstructure, the crack propagation mode was also primarily cleavage at -196°C. However, in contrast to the mild steel and Fe-3Si, the cleavage facets shown in Figure 10 are smaller, more irregular, and generally not as well defined. Areas of ductile tearing were also evident. In profile, Figure 11, the crack was found to exhibit occasional discontinuities over most of its length. The crack shown in Figure 11 propagated in a relatively stable manner by very small but rapid increases in length. The final propagation before the specimen was sectioned extended the crack approximately 0.10 inches. Near the crack tip, the crack path becomes quite discontinuous. Progressive sectioning in very small increments ($\sim$ 0.0004 in.) revealed that the crack surface in the A-517, like the Fe-3Si, is continuous and surrounds the unbroken ligaments. It would appear that in the case of A-517, these ligaments rupture at relatively small crack opening displacements since they are confined primarily to the crack-tip region. Exactly the same behavior is evident in the 4340 as can be seen in Figure 12. Here the crack propagated in a very unstable manner (at -196°C) for approximately 2 in. before arresting with a microcrack array at the tip.

Plastic Deformation During Propagation. By giving the Fe-3Si specimens a low temperature (150°C) anneal, dislocations are decorated with carbon and nitrogen. During subsequent etching, the decorated dislocations are preferentially attacked which thereby permits observation of deformation zones. A detailed discussion of the specimen preparation, aging, and etching procedures for displaying deformation in Fe-3Si can be found in Reference 16. Here it is pointed out that this technique is sufficiently sensitive to reveal individual dislocations when the plastic strains are small. As the plastic strain increases, the dislocations become so numerous that the area appears black. With further increases in plastic strain beyond 5 to 10%, the material no longer etches due to insufficient carbon to adequately decorate the dislocations. Therefore, crack-tip plastic zones are delineated by two boundaries: an outer one of essentially zero strain and an inner boundary within which the plastic strain exceeds 5 to 10%.

In Figure 13, are shown a series of macrographs which illustrates the increase with temperature of the extent of deformation on the surface of specimens tested at -75°C, 0°C, and 100°C. The plastic zones extending on either side of the crack are similar in size for both the 0°C and -75°C test temperatures. At 100°C, the plastic zone size is considerably larger consistent with the increased K_Q/Y. Accompanying this transition to a more ductile fracture mode is the development of shear lips and the tunneling of the crack along the midthickness.

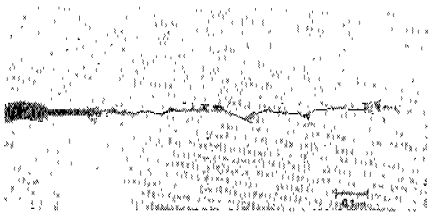

(a) -75°C

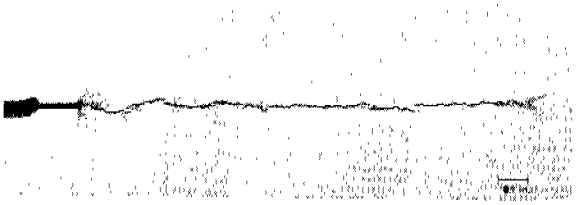

(b) 0°C

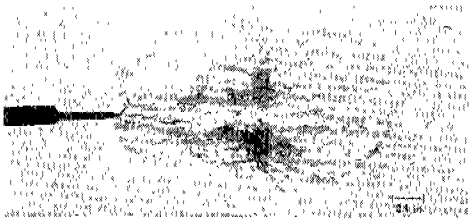

(c) 100°C

Fig.13. DEVELOPMENT OF SURFACE DEFORMATION WITH INCREASING TEST TEMPERATURE IN Fe-3Si

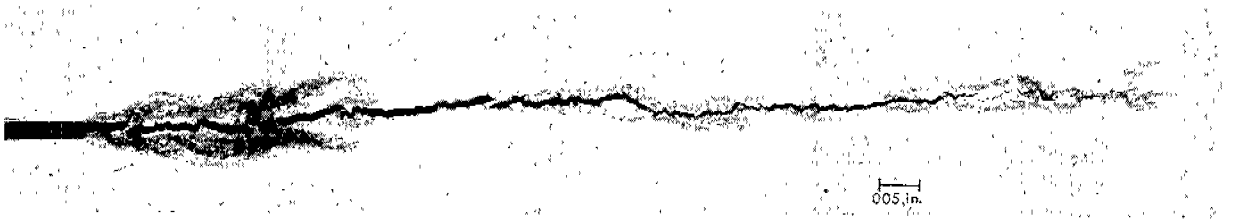

(a) Surface

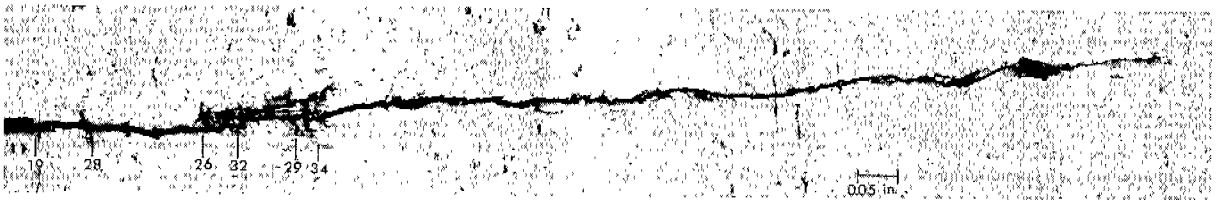

(b) Midthickness

Fig.14. COMPARISON OF THE DEFORMATION AT THE SURFACE AND MIDTHICKNESS OF A SPECIMEN TESTED AT 22°C. THE INITIATION-ARREST LOCATIONS ARE INDICATED IN THE MIDTHICKNESS VIEW BY THE K AT WHICH PROPAGATION OCCURRED

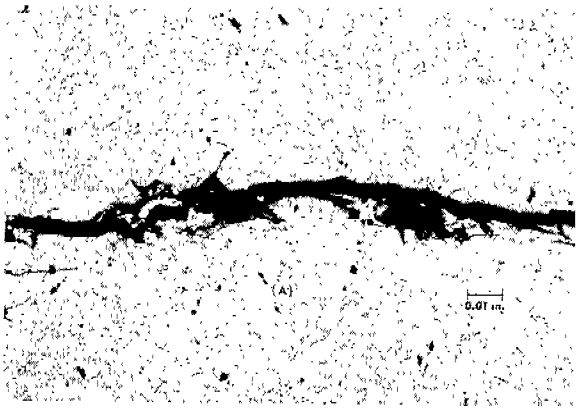

(a) 0.6 in. from crack tip

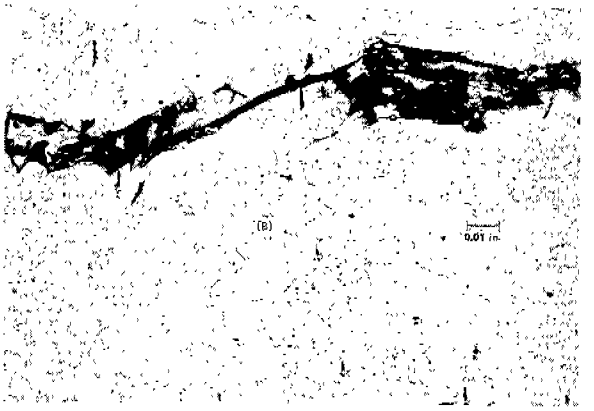

0.25 in. from crack tip

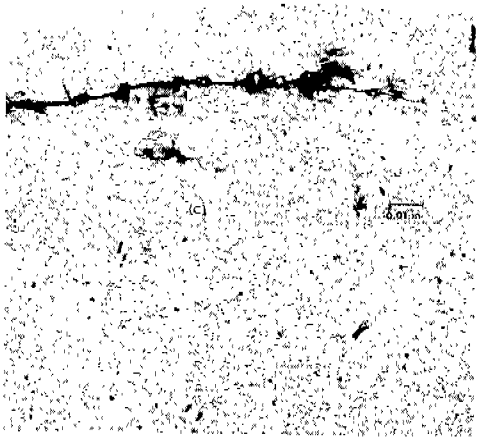

(c) arrested crack tip

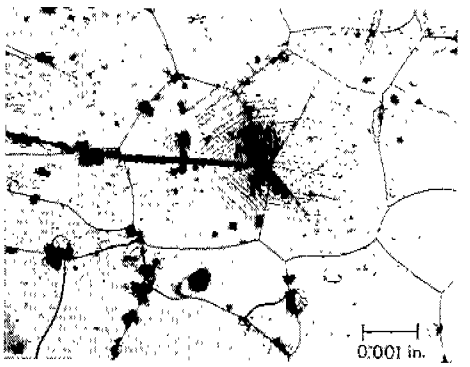

(d) crack tip

(d) Enlargement of the tip region of Fig.15(c) showing arrest at a grain boundary and subsequent deformation within the two adjacent grains

Fig.15. REGION OF UNSTABLE CRACK PROPAGATION IN SPECIMEN SHOWN IN Fig.14

Figure 14 shows a comparison of the surface deformation with the deformation at the midthickness position in a DCB specimen tested at 22°C. In this specimen, the crack propagated in short increments starting at 19 ksi $\sqrt{in.}$ from the 0.007 in.-wide slot and continued to propagate at a K level in the range of 27 to 32 ksi $\sqrt{in.}$ Each of the locations where arrest and reinitiation occurred is identifiable in the midthickness view by a plastic zone. Finally, at a K of 34 ksi $\sqrt{in.}$ at the crack length indicated in Figure 14, the propagation became very unstable and the crack ran the remaining distance. In Figure 14, there is evidence of considerable crack division resulting in fairly extensive unbroken regions just prior to the point at which initiation occurred at the K of 34 ksi $\sqrt{in.}$ As unbroken ligaments may interfere with propagation, a point discussed in more detail later, their presence at the crack tip increases the initiation threshold. This is an effect equivalent to increasing the root radius of the starter slot.

On the surface where plane stress conditions predominate and small shear lips are tending to form, the relatively uniform deformation along the first portion of the path suggests that crack extension here is continuous. In the unstable portion, the plastic zone is much smaller and in some areas has completely disappeared. Near the tip, unbroken regions within which relatively intense plastic strains have occurred are indicated by the areas which have etched white. At the midthickness position, in Figures 15a, b, and c, plastic deformation is apparently confined to the arrest-initiation locations and within and surrounding unbroken ligaments which occur at fairly random locations along the crack path. An excellent example of the crack tip deformation which occurred after arrest, and which results from the residual load on the specimen applied by the wedge, is shown in the magnified view in Figure 15d. These observations are identical to those made on other Fe-3Si specimens tested at room temperature and below and additional examples can be found in Figures 6 and 7 in Section 2 of this report.

These results suggest that virtually no plastic deformation occurs at the crack tip while it is moving. However, there is a small uncertainty in the extent of plastic deformation introduced by the small amount of material removed from the corners of the crack during etching. As the etching should remove no more than 0.001 in. from the crack, we may take this dimension as an upper limit to the plastic zone size in the fast crack regions. In Section I, it was found that the plastic zone size varied as

$$\rho = 0.13 \left(\frac{K}{Y}\right)^2$$

in the DCB specimen. Therefore, during rapid propagation $K/Y < 0.09 \sqrt{in.}$ at the crack tip. Near the arrested crack tip where the uncertainty in the extent of deformation due to etching is small, $K/Y < 0.04 \sqrt{in.}$ The plastic zone at the arrested tip in Figure 15d provides the measure of the arrest stress intensity as 7.7 ksi $\sqrt{in.}$ taking the static yield strength to be 62.4 ksi. However, the unbroken regions spanning the crack interface may support a portion of the applied load and, therefore, the applied stress intensity could be larger than this.*

* The arrested crack length in this specimen is outside the range of applicability of Equation (6).

IV. DISCUSSION

The ratio K_a/K_Q divides the DCB test results into two regimes. The property of stable crack propagation has been attached to those results in which K_a/K_Q is very nearly unity. In all other tests, K_a/K_Q was about 0.4 or less and here the term unstable propagation was applied. Crack propagation behavior yielding K_a/K_Q values in the range between these two extremes was not observed. From a macroscopic standpoint, crack propagation instability appears to develop very rapidly as K_Q increases. A simple energy balance offers a means of rationalizing these results and also provides a way of estimating the energy absorption rate from a comparison of K_a with K_Q.

During propagation, the energy release from the elastic strain field in the specimen is expended as kinetic energy and irreversible processes, the principal one being plastic deformation. The resulting energy balance is a modified Griffith-Orowan relation

$$\frac{dW}{da} = \frac{dU}{da} + R + \frac{dT}{da} \tag{8}$$

where T is the kinetic energy and U is the strain energy in the specimen. The left side of Equation (8) represents the rate of work done on the specimen during propagation. The crosshead travel is negligible during the short time period of propagation and as the elastic relaxation of the loading pins, wedge, and testing machine is also small, we can, as a first approximateion, set $dW/da = 0$. For consistency we have used the symbol R to represent energy dissipated during cracking but, in fact, R and G can be used interchangeably in keeping with formal definitions[23]. In the instant prior to the onset of propagation, while the kinetic energy is still zero, the familiar condition for fracture results, i.e., $dU/da = -R \equiv G_c$. Also, note that dU/da and R have opposite signs and for the magnitude of dU/da greater than the magnitude of R the kinetic energy must increase with increasing crack length. The interdependence between the three energy terms is shown schematically in Figure 16 where the dependence of R on crack length has been assumed. Actually, R is related to crack length only indirectly since

$$R = R(v)$$

and (9)

$$v = v(a)$$

where v is the crack velocity. An important point made in Figure 16 is that the kinetic energy in the system is not an energy sink term, i.e., kinetic energy may also be expended indirectly as deformation. Therefore, at the second point where $\frac{dU}{da}$ again equals R, the kinetic energy is maximum and for a further increase in crack length $R > \frac{dU}{da}$, $\frac{dT}{da} < 0$. The kinetic energy supplies the energy deficit to continue the expansion of the crack. The condition of arrest corresponds to T = 0 which from Equation (8) yields

$$\int_{a_o}^{a_f} dU = \int_{a_o}^{a_f} R\, da \tag{10}$$

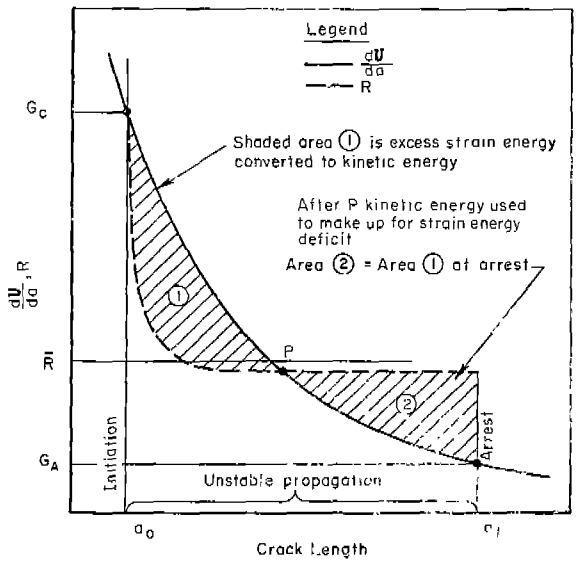

Fig.16. SCHEMATIC REPRESENTATION OF THE ENERGY CHANGES ACCOMPANYING PROPAGATION AND ARREST IN A DCB SPECIMEN. The $\frac{dU}{da}$ curve corresponds to crack growth under fixed-displacement conditions. The R-curve is hypothetical

where a_o and a_f are the initial and final crack lengths, respectively. In arriving at Equation (10), it is assumed that the system (the specimen and loading mechanism) is conservative (isolated) except only for heat lost through the crack plane during propagation. This assumption essentially requires that all kinetic energy is dissipated along the crack plane. To proceed further requires knowledge of the dependence of R upon crack velocity. When viewed on a macroscopic scale, the etching results show that the deformation is fairly uniform along the crack path. The deformation accompanying crack propagation appears to show a dependence on crack velocity only at the specimen surface when shear lips begin to form at the higher test temperatures. Therefore, as a reasonable first approximation, we can set

$$R = \begin{cases} R_Q = G_Q & v = 0 \\ R_d & v > 0 \end{cases} \tag{11}$$

where R_d is constant. Equation (10) becomes

$$R_d = \frac{1}{a_f - a_o} \int_{a_o}^{a_f} dU \tag{12}$$

Substituting Equation (6) and recalling that $G = K^2/E$, integration of 12 gives

$$R_d = \frac{1}{3}\left[G_Q^{1/2} + G_Q^{1/4} G_a^{1/4} + G_a^{1/2}\right]\left[G_Q^{1/4} G_a^{1/4}\right]$$

or

$$\frac{ER_d}{K_Q^2} = \frac{1}{3}\left[\left(\frac{K_a}{K_Q}\right)^{1/2} + \frac{K_a}{K_Q} + \left(\frac{K_a}{K_Q}\right)^{3/2}\right] \tag{13}$$

It can be recognized from Equation (12) that R_d falls between G_Q and G_a. Values of R_d calculated from Equation (13) and expressed in stress intensity units for A-517 steel are given in the following table.

TABLE 3. TABULATION OF K_Q, K_a, AND R_d VALUES FOR A-517 AT -196°C

Slot Diameter (in.)	K_Q (ksi$\sqrt{in.}$)	K_a (ksi$\sqrt{in.}$)	$\sqrt{ER_d}$ (ksi$\sqrt{in.}$)
Sharp	32 (K_{Ic})	31	31
0.007	42	18	28
0.009	43	12	24
0.025	69	16	36

Compared to the range of K_Q and K_a represented in this table, R_d is reasonably constant and approximately equal to G_{Ic}. The data also suggest the R_d may increase for very large K_Q which raises the question that R_d may be somewhat dependent on crack velocity. High speeds may attend large overstressing in turn causing an increase in R_d in the manner suggested by Eftis and Krafft[7]. However, this trend requires verification.

On the basis that $R_d \sim G_{Ic}$, predictions of the dependence of K_a on K_Q for all four steels can be made from Equation (13). Two conditions: $R_d = G_{Ic}(ER_d = K_{Ic}^2)$, and $R_d = 2/3\ G_{Ic}(ER_d = 2/3\ K_{Ic}^2)$ have been assumed and the resulting variation of K_a with K_Q are compared with the data in Figure 5. These predictions provide a fair representation of the data for all the steels, although the condition that $R_d = G_{Ic}$ appears to overestimate R_d. Additional data are needed to resolve the dependence of the ratio R_d/G_{Ic} on composition, microstructure, and temperature.

The data of Shoemaker and Rolfe for A-517 steel at -196°C give $K_{Ic}(\text{dynamic})/K_{Ic}(\text{static}) \sim 0.8$, a value which is nearly equal to the ratio $\sqrt{ER_d}/K_{Ic}$ for $R_d = 2/3\ G_{Ic}$. This suggests that, within the assumptions employed in arriving at Equations (11) and (13), the sharp crack dynamic toughness corresponds to the stress intensity required to sustain propagation. This does not mean, however, that for a given flaw size, a stress level which provides a $K \leq \sqrt{ER_d}$ is incapable of causing unstable catastrophic propagation in a structure. In particular if the structure is stressed such that K increases with increasing crack length, then a flaw originating in a small brittle region may enter the tougher surroundings and continue to grow even though its stress intensity at the instant it enters the matrix is $\leq \sqrt{ER_d}$. For example, consider the case of a large plate dead-weight-loaded in tension with a brittle region at the center. If a small crack initiates within and grows rapidly through the brittle zone, then at the instant the crack enters the surrounding "good" material, its size and the applied stress level define a K. For the crack to arrest, it is easily shown that R_d for the good material must satisfy $ER_d > 2K^2$. If this inequality is not satisfied, continued propagation is energetically favored.

At high magnifications, the etching results also show that $R_d \ll K_a^2/E$ except around the ligaments. Therefore, it appears that the major portion of the energy of propagation is expended within the unbroken ligaments behind the crack tip. If plastic deformation during propagation is confined primarily to unbroken regions behind the tip, then these ligaments must also support a significant portion of the applied load. Hence, the stress intensity at the crack tip will be less than the applied stress intensity. A solution which affords a useful estimate of this effect is obtained in Appendix A for the case of an infinite center-cracked plate loaded

along the crack plane by a finite number of point forces. From this analysis, the crack-tip stress intensity is given by

$$K = K_A - \frac{2F}{\sqrt{\pi a}} G(m,d)$$

where K_A is the applied stress intensity, F is the average force exerted by each ligament, m is the number of unbroken ligaments and d is the fraction of the crack length (2a) over which the ligaments remain unbroken (cf. Figure A-1). The function G(m,d) is plotted in Figure A-2 for a range of values of m and d.

Measurements of the ligament spacing and diameters along unstable cracks in the Fe-3Si in sections near the midthickness, indicate that the spacing ranges from about 0.005 in. to about 0.060 in. with an average of 0.022 in. and that the diameters vary in the range 0.002 to 0.020 in. averaging 0.007 in. Since the grain diameter in this steel is approximately 0.003 in. the ligaments involve roughly one to ten grains. Furthermore, taking the ligaments to be roughly circular and equidistant, the areal fraction of unbroken ligaments is about 0.1. The distance back from the crack tip where unbroken ligaments could be found ($a-\ell$) averages 0.44 in. As the ligament model is strictly two dimensional, it is necessary to rearrange the ligament array on the surface into an equivalent pattern of unbroken strips extending across the specimen thickness. On this basis, the strip spacing would be one-half the observed ligament spacing and the area of each unbroken strip is, for a specimen thickness of 0.5 in., 5.5×10^{-4} in.^{2} . The ligaments are subject to considerable restraint and high strain rates and, therefore, a reasonable estimate of the flow stress prior to rupture is 150 ksi. For a crack length of about 2 in., we find

$$F = 82.5 \text{ lbf}$$

$$d = 0.22$$

$$m = 40$$

$$G(m,d) \simeq 160$$

and

$$\frac{2F}{\sqrt{\pi a}} G(m,d) \simeq 10 \text{ ksi} \sqrt{\text{in.}}$$

As a "ballpark" estimate, this result is very significant as it implies that the ligaments could successfully unload the crack tip. Furthermore, since this calculation is based upon measurements along the midthickness profile, it should underestimate the actual reduction in crack-tip stress intensity since the ligaments near the surfaces are apparently larger and more closely spaced.

The results of the above model serve to emphasize the importance of the unbroken ligaments on propagation behavior. If the ligaments act to produce a significant difference between the applied K and the crack-tip K, then also the ligaments must provide an important sink for energy dissipation during propagation. Therefore, a major part of R_d can now be attributed to deformation and rupture of unbroken areas as the crack extends, direct evidence for which was available only in the case of the Fe-3Si etching results.

In summary, the etching results coupled with the energy balance and ligament model analyses provide evidence that the source of the resistance to rapid crack propagation is not in the crack-tip region but rather unbroken regions which are bypassed as the crack grows. This conclusion seems applicable at least to the steels and

testing conditions employed in this study. The source of the ligaments is not yet clear although two possibilities exist: anomolously tough regions which are scattered randomly throughout the steel, or a region of one or more grains whose cleavage planes are poorly oriented while the surrounding grains are well oriented for propagation.

The wedge-loaded DCB test used in this study provides a very useful means of studying crack propagation as the entire spectrum of propagation stability can be examined. Indeed, the ability to achieve stable propagation is attributable to the inherent stiffness of the loading system. Furthermore, these tests indicated that on the basis of the arrest toughness, the apparent resistance to crack propagation is dependent upon the initiation conditions. Therefore, K_a is not, by itself, a test independent indicator of crack propagation resistance.

Finally, there are many aspects of rapid crack propagation which have not been considered here. In particular, elastic wave effects such as reflections from free surfaces back to the crack tip may play an important role in propagation. While quasi-static analyses of crack propagation have been developed, a fully dynamic treatment of crack propagation would be enormously difficult. The evaluation of such effects is more realistically attacked from the experimental standpoint.

V. CONCLUSIONS

1. The inherent stiffness of the wedge-loaded DCB test affords a means of propagating a crack in a relatively stable manner such that the stress intensity at initiation (K_Q) and arrest (K_a) are very nearly equal. By increasing K_Q through increasing the root radius of the starter slot, K_a undergoes an abrupt decrease to $K_a/K_Q \leq 0.4$ for steels with a wide range of yield strengths from 62 ksi to 310 ksi.

2. During cleavage propagation, the crack advances in a nonplanar fashion generating unbroken regions or ligaments randomly. These ligaments may remain unbroken for considerable distances behind the crack front. This observation is essentially the same whether the crack is propagating in a stable or unstable fashion. Furthermore, completely isolated microcracks are rare.

3. On the average, no gross discontinuities in the deformation during propagation were evident on a macroscopic scale from the etching studies. Therefore, as a first approximation, the dynamic energy absorption rate, R_d, was taken to be independent of velocity. An energy balance of propagation indicates that the average R_d is approximately 2/3 G_{Ic} or $\sqrt{ER_d} \simeq 0.8\ K_{Ic}$ for the steels and testing conditions in this study. The ratio $\sqrt{ER_d}/K_{Ic}$ is also very nearly equal to $K_{Ic}(\text{dynamic})/K_{Ic}(\text{static})$ obtained by Shoemaker and Rolfe for similar materials.

4. Deformation associated with the crack tip during cleavage propagation could not be resolved. Therefore, propagation by cleavage, at least in the Fe-3Si steel, is nearly ideally brittle with $R_d(\text{tip})/G_{Ic} \leq 0.01$. The deformation is confined to the unbroken ligaments as the crack extends and the overall energy of propagation is primarily absorbed in their deformation and rupture.

5. An analysis of point forces distributed along a crack surface was used to model the ligaments joining the crack interfaces and thereby gain an estimate of the effect of these ligaments on the crack-tip stress intensity. Based on measurements of ligament size and spacing, this estimate indicates that the actual crack-tip stress intensity can be appreciably less than the applied stress intensity due to the load borne by the unbroken regions behind the crack tip. This analysis offers an independent check of the conclusion that the ligaments afford the principal energy absorbing sink during propagation.

VI. REFERENCES

1. T. S. Robertson, J. Iron and Steel Inst., p. 361, 1953.

2. Y. Akita and K. Ikeda, Transportation Tech. Research Inst., Report 56, Tokyo, December, 1962.

3. M. Yoshiki, T. Kanazawa, and S. Machida, Proc. Seventh Jap. Cong. Test. Mat., p. 71, 1964.

4. J. I. Bluhm, Fracture, an Advanced Treatise, H. Liebowitz, ed., Academic Press, New York, p. 1, 1969.

5. H. Itagaki, T. Kanazawa, and M. Yokhiki, Studies on the Brittle Fracture Problems in Japan, M. Yoshiki and T. Kanazawa, eds., Soc. of Naval Architects of Japan, 13, 1967, p. 72.

6. R. G. Hoagland, Trans ASME, Series D, Vol. 89, p. 525, 1967.

7. A. A. Wells, Welding Research, Vol. 7, p. 34, 1953.

8. R. Weichert and K. Schonert, Int. J. of Fracture Mech., Vol. 5, p. 353, 1969.

9. J. Eftis and J. M. Krafft, Trans ASME, Series D, Vol. 87, p. 257, 1964.

10. F. P. Videon, F. W. Barton, and W. J. Hall, SSC Report 148, 1963.

11. K. B. Broberg, Arkin för Fysik, Vol. 18, p. 159, 1960.

12. J. Dvorak, Fracture 1969, P. L. Pratt, et al, eds., Chapman and Hall, London, p. 338, 1969.

13. P. B. Crosley and E. J. Ripling, Trans ASME, Series D, Vol. 91, p. 525, 1969.

14. G. T. Hahn, W. S. Owen, B. L. Averbach, and M. Cohen, Welding J., September, 1959.

15. G. T. Hahn, B. L. Averbach, W. S. Owen, and M. Cohen, Fracture, Proc. Swampscott Conf., Wiley, New York, p. 91, 1959.

16. G. T. Hahn, P. N. Mincer, and A. R. Rosenfield, "The Fe-3Si Steel Etching Technique for Local Strain Measurement", submitted to Experimental Mechanics (to be published).

17. B. Gross and J. E. Srawley, NASA Technical Note, TN D-3295, February, 1966.

18. D. P. Clausing, Int. J. Frac. Mech., Vol. 5, p. 211, 1969.

19. W. F. Brown and J. E. Srawley, Plane Strain Crack Toughness Testing of High Strength Metallic Materials, ASTM STP 410, 1967.

20. A. K. Shoemaker and S. T. Rolfe, Trans ASME, Series D, Vol. 91, p. 512, 1969.

21. J. M. Krafft, NRL Progress Report, p. 4, November, 1963.

22. G. C. Sih, Inelastic Behavior of Solids, McGraw-Hill, New York, p. 607, 1970.

23. C. Atkinson and J. D. Eshelby, Int. J. of Fracture Mech., Vol. 4, p. 3, 1968.

ACKNOWLEDGMENTS

The authors are grateful to Ship Structure Committee for their support and to Advisory Group III of the Ship Research Committee (S. T. Rolfe, Coordinator) and to A. R. Lytle and R. W. Rumke of the Academy for valuable advice and encouragement. They are also indebted to M. Lightner of the U. S. Steel Corporation, who contributed the heat of T-1 steel used in this study. Experimental results for 4340 steel are derived from studies for the Army Research Office (Durham). The authors also wish to acknowledge the experimental assistance of R. L. Stephenson, and fruitful discussions with M. F. Kanninen. Valuable assistance in preparation of the manuscript was provided by Miss C. Pepper.

APPENDIX A

THE EFFECT OF CRACK-LINE TRACTIONS ON THE CRACK-TIP STRESS INTENSITY

If, as a crack grows, it encircles and leaves behind islands of unbroken material or ligaments, the stress intensity describing the stresses in the crack-tip region will become increasingly smaller than the applied stress intensity* as the unbroken ligaments become more numerous. The effect of these ligaments may be adequately treated by appealing to a simple two-dimensional analogue consisting of a large, center-cracked plate loaded along the crack plane by a series of point forces which simulate the ligaments (Figure A-1). Following the complex variable method of Muskhelishvili[1], we define a function, ϕ, in the complex z-plane such that

$$\sigma_{xx} + \sigma_{yy} = 2[\phi'(z) + \overline{\phi'(z)}]$$

We may consider the stress function ϕ as arising solely from the point force tractions along the crack plane. Then, if the plate is loaded in some fashion along its boundary to produce an applied stress intensity, K_A, the net stress intensity is

$$K = K_A + \lim_{\substack{x \to a \\ x > a}} [\phi'(z) + \overline{\phi'(z)}] \qquad y = o \qquad \text{(A-1)}$$

The conformal mapping

$$z = \frac{a}{2}\left(\xi + \frac{1}{\xi}\right)$$

transforms the unit circle in the ξ-plane into a slit of length 2a in the z-plane. In the ξ-plane, Muskhelishvili provides a solution for a distributed force over an arc of the circle. By allowing the arc length to decrease to zero such that the resulting point force, F, is finite, Muskhelishvili's solution reduces to

$$\phi(\xi) = -\frac{F}{2\pi i} \ln(\sigma - \xi)$$

where σ is the point along the hole boundary at which the force, F, is applied. For a distribution of n point forces on the crack plane except at the crack tips, $x = \pm a$,

$$\phi(\xi) = -\frac{1}{2\pi i} \sum_{j}^{n} F_j \ln(\sigma_j - \xi)$$

---

* The stress intensity based on the applied stress and crack length neglecting tractions along the crack surface.

A-2

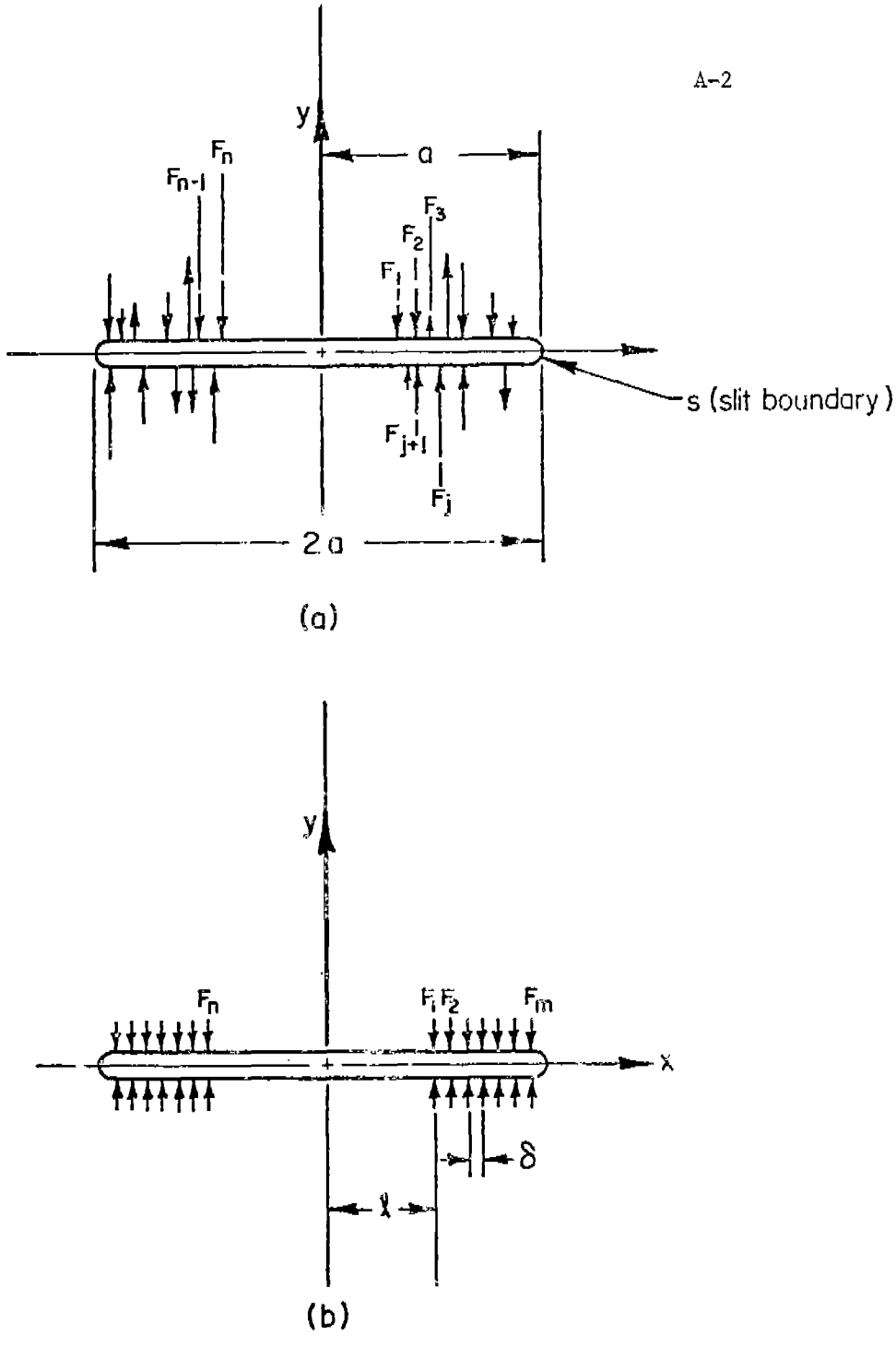

Fig.A-1. (a) CENTER-CRACKED SHEET LOADED BY POINT FORCES DISTRIBUTED RANDOMLY OVER THE SLIT BOUNDARY. THERE ARE N FORCES NUMBERED IN A CLOCKWISE FASHION.

(b) SAME AS (a) EXCEPT THAT THE FORCES ARE EQUAL AND UNIFORMLY SPACED

Equation (D-1) becomes

$$K = K_A - \frac{1}{2\sqrt{\pi a}} \sum_{j=1}^{n} F_j \frac{\sin\theta_j}{1-\cos\theta_j} \qquad (A-2)$$

where θ_j is defined by $x_j = \cos\theta$; and x_j is the location of the j^{th} force on the crack plane. Let us now examine the particular case in Figure A-1b of equal magnitude forces equally spaced a distance δ. The first force is positioned at $x_i = \ell$ and, making the substitution $d = (a-\ell)/a$, Equation (A-2) becomes

$$K = K_A - \frac{2F}{\sqrt{\pi a}} \sum_{j=1}^{m} \frac{m}{\sqrt{m^2-[m(1-d) + (j-1)d]^2}}$$

or more compactly

$$K = K_A - \frac{2F}{\sqrt{\pi a}} G(m,d) \qquad (A-3)$$

where $m = n/4$. The function $G(m,d)$ is plotted in Figure A-2. As $m \to \infty$, the force distribution becomes continuous and $\frac{\delta}{a} G(m,d)$ approaches $\cos^{-1}(1-d)$. Therefore, the term due to the ligaments on the right side of Equation (A-3) becomes, for large m (large number of ligaments)

$$\frac{2F}{\delta}\sqrt{\frac{a}{\pi}} \cos^{-1}(1-d)$$

which is precisely the result obtained by Dugdale[2] for a continuous stress $Y = F/\delta$ superposed along the crack surface near the crack tip.

References

1. N. I. Muskhelishvili, Some Basic Problems of the Mathematical Theory of Elasticity, Noordhoff, Holand, 1953.

2. D. S. Dugdale, J. Mech. Phys. Solids, Vol. 8, p. 100, 1960.

A-4

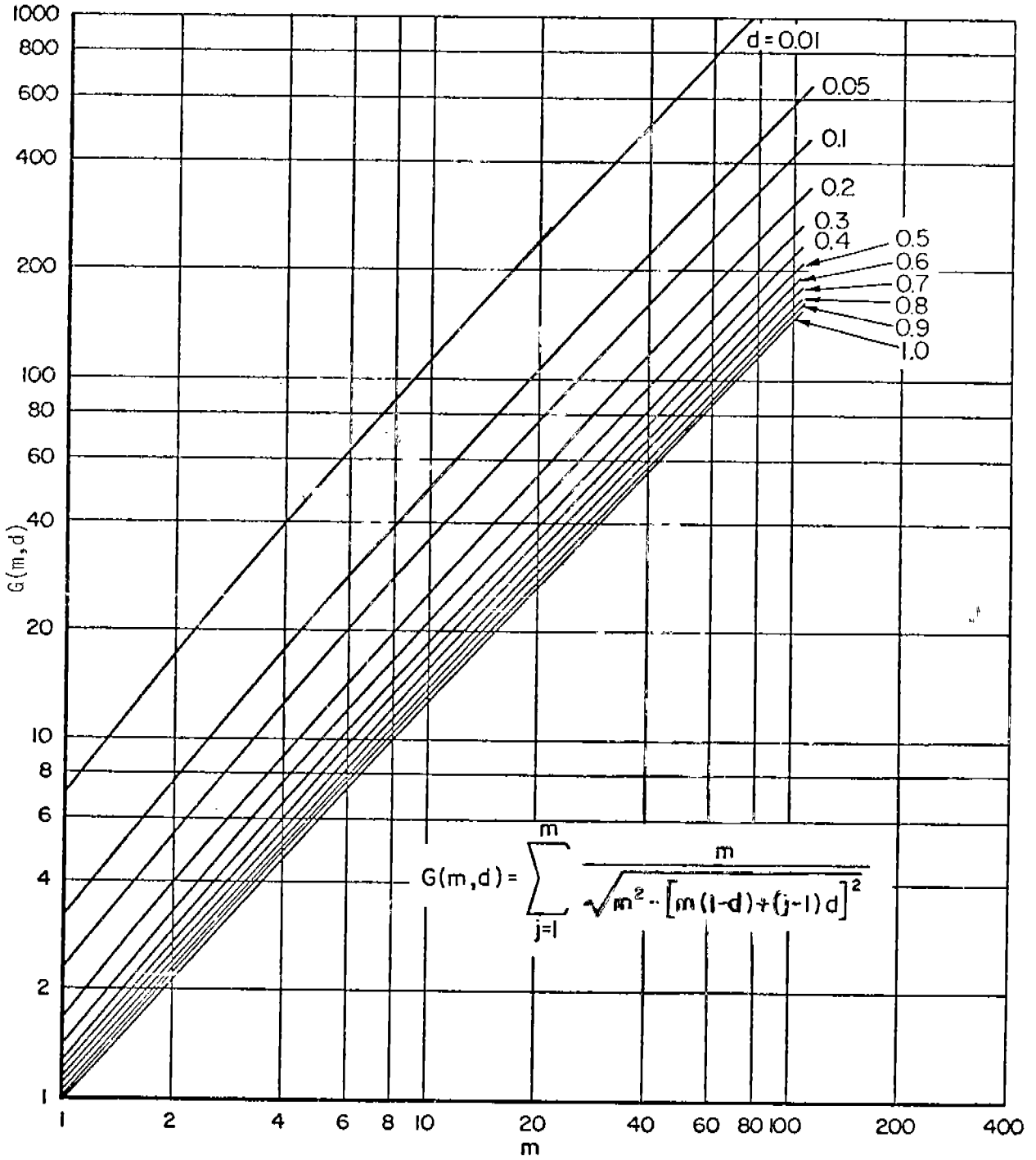

Fig. A-2. THE RESULTS OF THE ANALYSIS FOR THE UNIFORMLY SPACED EQUAL FORCE MODEL

None

Security Classification

DOCUMENT CONTROL DATA - R & D

(Security classification of title, body of abstract and indexing annotation must be entered when the overall report is classified)

1 ORIGINATING ACTIVITY *(Corporate author)* Battelle Memorial Institute Columbus, Ohio	2a. REPORT SECURITY CLASSIFICATION Unclassified 2b. GROUP

3. REPORT TITLE

CRACK PROPAGATION AND ARREST IN SHIP AND OTHER STEELS

4 DESCRIPTIVE NOTES *(Type of report and inclusive dates)*

5. AUTHOR(S) *(First name, middle initial, last name)*

G. T. Hahn, R. G. Hoagland, P. N. Mincer, A. R. Rosenfield, and M. Sarrate

6. REPORT DATE August, 1970	7a. TOTAL NO. OF PAGES 55	7b. NO. OF REFS 58
8a. CONTRACT OR GRANT NO. N00024-68-C-5073 b. PROJECT NO. SR-180 c. d.	9a. ORIGINATOR'S REPORT NUMBER(S) SSC-219 9b. OTHER REPORT NO(S) *(Any other numbers that may be assigned this report)*	

10. DISTRIBUTION STATEMENT

Distribution of this document is unlimited.

11 SUPPLEMENTARY NOTES	12. SPONSORING MILITARY ACTIVITY Naval Ship Engineering Center

13. ABSTRACT

This report describes a three-part investigation into the major stages of fracture--initiation, propagation, and arrest. A wedge-loaded double-cantilever-beam design was used on Fe-3Si Steel where crack-tip yielding can be revealed by a special etching technique. Additionally, a number of experiments were done on engineering steels, principally to study propagation resistance. It was found that the fast moving crack bypasses some of the grains as it grows, leaving behind ligaments. Rupture of these ligaments consumes a large amount of energy locally and this process can account for crack propagation resistance values estimated from these experiments. Upon increasing root radius of the initial notch, the crack must be overloaded to propagate, and a wide range of values of the crack driving force, G, can be obtained in a single experiment. This provides a new method of measuring crack propagation resistance, R. Etching results suggest that R does not vary greatly as the crack grows. An energy balance shows that R is the average value of G during propagation. By this means, partial confirmation is given to the idea that R is equal to the value of G_{Ic} measured in an impact test. It is then shown that the rate and temperature dependence of $K_{Ic} = (EG_{Ic})^{1/2}$ arises from the rate and temperature dependence of the yield stress in the crack-tip plastic zone. These analyses and experiments thus provide a framework for developing a practical arrest criterion for ship steels.

DD FORM 1 NOV 65 1473 (PAGE 1)

S/N 0101-807-6801

None

Security Classification

None
Security Classification

14 KEY WORDS	LINK A		LINK B		LINK C	
	ROLE	WT	ROLE	WT	ROLE	WT
Fracture Mechanics Fracture Toughness (K_{Ic}) Crack Initiation Crack Propagation Crack Arrest Structural Steel Plastic Zones of Crack Tips Double-Cantilever-Beam Specimen Cleavage Fracture of Steels Elastic-Plastic Analysis Fracture, Rate, and Temperature Effects						

DD FORM 1 NOV 65 1473 (BACK)
(PAGE 2)

None
Security Classification

GPO 917-317

SHIP RESEARCH COMMITTEE
Maritime Transportation Research Board
National Academy of Sciences-National Research Council

The Ship Research Committee has technical cognizance of the Ship Structure Committee's Research Program. This entails recommending research objectives, preparing project prospectuses, evaluating proposals, providing liaison and technical guidance, reviewing project reports, and stimulating productive avenues of research.

PROF. R. A. YAGLE, Chairman
Professor of Naval Architecture
University of Michigan

DR. H. N. ABRAMSON
Director, Dept. of Mechanical Sciences
Southwest Research Institute

MR. W. H. BUCKLEY
Chief, Structural Criteria and Loads
Bell Aerosystems Co.

DR. D. P. CLAUSING
Senior Scientist
U.S. Steel Corporation

MR. A. E. COX
Senior Program Manager
Newport News Shipbuilding & Dry Dock Co.

MR. J. F. DALZELL
Senior Research Engineer
Stevens Institute of Technology

DR. W. D. DOTY
Senior Research Consultant
U.S. Steel Corporation

MR. F. D. DUFFEY
Manager of Welding & Methods
Maryland Shipbuilding & Dry Dock Co.

MR. D. FAULKNER
Research Associate
Massachusetts Institute of Technology

PROF. W. J. HALL
Professor of Civil Engineering
University of Illinois

MR. J. E. HERZ
Chief Structural Design Engineer
Sun Shipbuilding & Dry Dock Co.

MR. G. E. KAMPSCHAEFER, JR.
Manager, Application Engineering
ARMCO Steel Corporation

PROF. B. R. NOTON
Prof. of Aerospace & Civil Engineering
Washington University

MR. W. W. OFFNER
Consulting Engineer

CDR R. M. WHITE, USCG
Chief, Applied Engineering Section
U.S. Coast Guard Academy

MR. R. W. RUMKE
Executive Secretary
Ship Research Committee

This project was coordinated under the guidance of the following Advisory Group III, "Metallurgical Studies" membership:

PROF. W. J. HALL, Chairman, *Prof. of Civil Engineering, University of Illinois*
DR. D. P. CLAUSING, *Senior Scientist, U.S. Steel Corporation*
DR. W. D. DOTY, *Senior Research Consultant, U.S. Steel Corporation*
MR. F. D. DUFFEY, *Manager of Welding & Methods, Maryland Shipbuilding & Dry Dock Co.*
MR. G. E. KAMPSCHAEFER, JR., *Manager, Application Engineering, ARMCO Steel Corp.*
MR. W. W. OFFNER, *Consulting Engineer*
PROF. A. W. PENSE, *Prof. of Metallurgy, Lehigh University, Bethlehem, Pa.*

SHIP STRUCTURE COMMITTEE PUBLICATIONS

These documents are distributed by the National Technical Information Service, Springfield, Va. 22151. These documents have been announced in the Clearinghouse journal U.S. Government Research & Development Reports (USGRDR) under the indicated AD numbers.

SSC-206, *Permissible Stresses and their Limitations* by J. J. Nibbering. 1970. AD 710520.

SSC-207, *Effect of Flame and Mechanical Straightening on Material Properties of Weldments* by H. E. Pattee, R. M. Evans, and R. E. Monroe. 1970. AD 710521.

SSC-208, *Slamming of Ships: A Critical Review of the Current State of Knowledge* by J. R. Henry and F. C. Bailey. 1970. AD 711267.

SSC-209, *Results from Full-Scale Measurements of Midship Bending Stresses on Three Dry Cargo Ships* by I. J. Walters and F. C. Bailey. 1970. AD 712183.

SSC-210, *Analysis of Slamming Data from the "S. S. Wolverine State"* by J. W. Wheaton, C. H. Kano, P. T. Diamant, and F. C. Bailey. 1970. AD 713196.

SSC-211, *Design & Installation of a Ship Response Instrumentation System Aboard the Container Vessel "S. S. Boston"* by R. A. Fain, J. Q. Cragin and B. H. Schofield. (To be published).

SSC-212, *Ship Response Instrumentation Aboard the Container Vessel "S. S. Boston": Results from the 1st Operational Season in North Atlantic Service* by R. A. Fain, J. Q. Cragin, and B. H. Schofield. 1970. AD 712186.

SSC-213, *A Guide for Ultrasonic Testing and Evaluation of Weld Flaws* by R. A. Youshaw. 1970. AD 713202.

SSC-214, *Ship Response Instrumentation Aboard the Container Vessel "S. S. Boston": Results from Two Operational Seasons in North Atlantic Service* by J. Q. Cragin. 1970. AD 712187.

SSC-215, *A Guide for the Synthesis of Ship Structures Part One - The Midship Hold of a Transversely-Framed Dry Cargo Ship* by Manley St.Denis. 1970. AD 717357.

SSC-216, (To be published).

SSC-217, *Compressive Strength of Ship Hull Girders - Part I - Unstiffened Plates* by H. Becker, R. Goldman, and J. Pozerycki. 1971. AD 717590.

SSC-218, *Design Considerations for Aluminum Hull Structures: Study of Aluminum Bulk Carriers* by C. J. Altenburg and R. J. Scott. 1971.